ELSEVIER

Remote Sensing of Environment 76 (2000) 156–172

Remote Sensing of Environment

www.elsevier.com/locate/rse

# Comparing prediction power and stability of broadband and hyperspectral vegetation indices for estimation of green leaf area index and canopy chlorophyll density

N.H. Broge[a,*], E. Leblanc[b]

[a]*Department of Agricultural Systems, Danish Institute of Agricultural Sciences, Research Centre Foulum, P.O. Box 50, DK-8830 Tjele, Denmark*
[b]*USDA-ARS, Biometrical Consulting Service, 10300 Baltimore Avenue., Beltsville, MD, USA*

Received 8 December 1999; accepted 30 October 2000

**Abstract**

Hyperspectral reflectance data representing a wide range of canopies were simulated using the combined PROSPECT + SAIL model. The simulations were used to study the stability of recently proposed vegetation indices (VIs) derived from adjacent narrowband spectral reflectance data across the visible (VIS) and near infrared (NIR) region of the electromagnetic spectrum. The prediction power of these indices with respect to green leaf area index (LAI) and canopy chlorophyll density (CCD) was compared, and their sensitivity to canopy architecture, illumination geometry, soil background reflectance, and atmospheric conditions were analyzed. The second soil-adjusted vegetation index (SAVI2) proved to be the best overall choice as a greenness measure. However, it is also shown that the dynamics of the VIs are very different in terms of their sensitivity to the different external factors that affects the spectral reflectance signatures of the various modeled canopies. It is concluded that hyperspectral indices are not necessarily better at predicting LAI and CCD, but that selection of a VI should depend upon (1) which parameter that needs to be estimated (LAI or CCD), (2) the expected range of this parameter, and (3) a priori knowledge of the variation of external parameters affecting the spectral reflectance of the canopy. 

## 1. Introduction

Spectral reflectance of vegetation in the visible (VIS) region of the electromagnetic spectrum is primarily governed by chlorophyll pigments (Thomas & Gausman, 1977). Developments within the field of hyperspectral remote sensing imaging sensors have allowed for new ways of monitoring plant growth and estimating potential photosynthetic productivity.

Many studies have focused on the relationship between pigment concentration and optical properties of leaves (Horler, Dockray, & Barber, 1983; Jacquemoud et al., 1996; Lichtenthaler, Gitelson, & Lang, 1996). A number of investigators have studied the relationship between canopy spectral reflectance and canopy characteristics for major crops (Baret, Champion, Guyot, & Podaire, 1987; Gilabert, Gandia, & Melia, 1996; Jackson & Pinter, 1986). For example, spectral vegetation indices (VIs) calculated as linear combinations of near infrared (NIR) and VIS red reflectance have been found to be well correlated with canopy cover, leaf area index (LAI), and absorbed photosynthetically active radiation (APAR) (Elvidge & Chen, 1995; Myneni & Williams, 1994). However, it has been shown that most traditional VIs are sensitive to soil background, especially at low LAIs (Huete, 1989; Huete, Jackson, & Post, 1985).

The wavelength region located in the VIS–NIR transition has been shown to have a high information content for vegetation spectra (Collins, 1978; Horler, Dockray, & Barber, 1983). The spectral reflectance of vegetation in this region is characterized by very low reflectance in the red part of the spectrum followed by an abrupt increase in reflectance at 700–740 nanometer (nm) wavelengths. This spectral reflectance pattern of vegetation is generally referred to as the "red edge." Several studies have shown that measures based on the red edge position or shape are likewise well correlated with biophysical parameters at the canopy level, but less sensitive to spectral noise caused by

* Corresponding author.
*E-mail address*: nielsh.broge@agrsci.dk (N.H. Broge).

0034-4257/00/$ – see front matter 
PII: S0034-4257(00)00197-8

the soil background and by atmospheric effects (Baret, Jacquemoud, Guyot, & Leprieur, 1992; Demetriades-Shah, Steven, & Clark, 1990; Guyot, Baret, & Jacquemoud, 1992; Mauser & Bach, 1995).

The objective of the present study is to compare different VIS–NIR spectral reflectance-based approaches for estimation of LAI and canopy chlorophyll density (CCD). As part of this assessment the effects of the soil background and the atmosphere are considered. The analyses are based on simulated canopy spectral reflectance data using acknowledged radiative transfer models in combination with real soil reflectance data.

The study is composed of three phases addressing (1) the effects of structural and biochemical variation in the canopy, (2) the effects of variations in soil background reflectance, and (3) the effects of varying atmospheric conditions. A canopy reflectance database was created for each phase of the study.

## 2. Canopy reflectance simulations

Canopy spectral reflectance was simulated using the PROSPECT leaf optical model (Baret et al., 1992; Jacquemoud & Baret, 1990) coupled with the Scattering by Arbitrarily Inclined Leaves (SAIL) canopy reflectance model (Verhoef, 1984) modified to include the hot spot effect (Kuusk, 1991). The SAIL model is an analytical, physically based four-stream radiative transfer model that considers the canopy a homogeneous, infinitely extended vegetation layer made up of leaves distributed at random. The leaves are considered perfect Lambertian scatterers and assumed to have a random distribution in terms of azimuth angle. The leaf zenith angle distribution is considered ellipsoidal, characterized by the mean leaf inclination angle. PROSPECT is a leaf optical properties model that estimates leaf reflectance and transmittance from other leaf characteristics. The model idealizes the leaf as a stack of identical elementary layers defined by a refractive index and an absorption coefficient, and assumes that all leaf components are distributed homogeneously within the leaf. Both of these models have proven very stable and generate accurate results whilst being relatively simple in terms of the number of input parameters needed (Goel & Thompson, 1984; Jacquemoud, Baret, Andrieu, Danson, & Jaggard, 1995; Jacquemoud et al., 1996). The combined SAIL + PROSPECT model (Jacquemoud, 1993) calculates canopy spectral reflectance computed from the following input parameters:

- Biophysical parameters: Leaf chlorophyll $a+b$ concentration, $C_{ab}$ ($\mu g/cm^2$); Leaf mesophyll structure, $N$; Leaf water depth, $C_w$ (cm); Leaf dry matter content, $C_{dm}$ ($g/cm^2$); Green leaf area index, LAI; Leaf mean tip angle, MTA.
- Soil spectral reflectance, $\rho_s(\lambda)$.
- External parameters: Solar zenith and azimuth angle, $\theta_s$ (°) and $\psi_s$ (°); View zenith and azimuth angles, $\theta_v$ (°) and $\psi_v$ (°); Fraction of incident diffuse skylight expressed in terms of visibility, Vis (km); The Kuusk hot spot size parameter, $s$.

The mathematical form of the combined model is given by Eq. (1):

$$\rho(\lambda) = f(\theta_s, \psi_s, \theta_v, \psi_v, MTA, LAI, N, C_{ab}, C_w, C_{dm}, s, Vis, \rho_s(\lambda)) \quad (1)$$

where $\rho$ is reflectance at wavelength $\lambda$.

Three canopy spectral reflectance databases were constructed to investigate the effects of:

1. canopy architecture and composition (Canopy effects),
2. background spectral reflectance (Background effects), and,
3. atmospheric composition (Atmospheric effects).

Leaf water content governs the reflectance properties beyond 1000 nm, but has practically no effect on the spectral properties in the VIS and NIR regions. Variations of leaf dry matter content affects canopy reflectance by increasing or decreasing the multiple intercellular scattering of the NIR rays. However, for practical remote sensing applications, this effect can be assumed to be negligible, because the within-crop variation of leaf dry matter content is very stable. The leaf structure parameter was fixed at 1.5 in the simulations, which according to Jacquemoud and Baret (1990) corresponds to most plant leaves. Only nadir view angle ($\theta_v = 0$) was considered. LAI is a key variable frequently used as input for crop growth models and soil–vegetation–atmosphere-transfer (SVAT) models. It is functionally linked with the evolution of canopy spectral reflectance over the growth season. For these reasons, all three databases are constructed from simulations where LAI is adjusted as the controlling variable. The photosynthetic potential of the plants is primarily controlled by the concentration of chlorophyll pigments, which are intimately involved in the photosynthetic process. The CCD is a measure of photosynthetic potential at the canopy level and is calculated as the product of the model input parameters LAI and $C_{ab}$. The parameters used to establish the canopy reflectance databases are summarized in Table 1.

### 2.1. Canopy effects

Canopy reflectance in the VIS and NIR has been shown to be affected not only by LAI and pigment concentration but also by canopy architecture, illumination and viewing geometry (Jackson & Pinter, 1986; Pinter, Jackson, Ezra, & Gausman, 1985). These effects were considered in the model simulations by changing the leaf chlorophyll content,

Table 1
Parameter values used to establish the canopy reflectance databases

| Model parameters | Database 1, Canopy effects | Database 2, Background effects | Database 3, Atmospheric effects |
|---|---|---|---|
| LAI ( − ) | 0.1, 0.2, 0.4, 0.8, 1.6, 2.4, 3.2, 4.0, 4.8, 6.4, 9.6, 12.8 | 0.1, 0.2, 0.4, 0.8, 1.6, 2.4, 3.2, 4.0, 4.8, 6.4, 9.6, 12.8 | 0.1, 0.2, 0.4, 0.8, 1.6, 2.4, 3.2, 4.0, 4.8, 6.4, 9.6, 12.8 |
| $C_{ab}$ (μg/cm$^2$) | 20, 30, 40, 50, 60, 70, 80 | 50 | 50 |
| $\theta_s$ (°) | 15, 30, 45, 60 | 45 | 45 |
| MTA (°) | 30, 40, 50, 60, 70 | 50 | 50 |
| $\rho_s(\lambda)$[a] ( − ) | $a_w$ | $a_w$, $a_d$, $b_w$, $b_d$, $c_w$, $c_d$, $d_w$, $d_d$, $e_w$, $e_d$ | $a_w$ |
| Atmospheric $H_2O$ (cm) | 3 | 3 | 1.5, 3.0, 4.5 |
| Atmospheric $\tau_{550}$ ( − ) | 0.3 | 0.3 | 0.05, 0.3, 1.0 |

[a] The subscript ('w' or 'd') refers to the wetness of the soil, i.e. wet or dry.

the leaf mean tip angle, LAI+ and the solar zenith angle. The range of these parameter values was selected to represent a broad range of canopies, according to Table 1. The resulting database holds simulated canopy spectral reflectance data for 1,680 different canopies.

### 2.2. Background effects

A study of prediction power and sensitivity to external factors, which in this context includes all factors other than LAI or CCD, should also include sensitivity to noise induced by variations in the background reflection. This was accomplished by simulation of a new set of spectra using measured spectral reflectance properties of each of five spectrally distinct soils as the lower boundary reflectance in the simulations. The soil reflectance database was created from topsoil samples of five U.S. cropland soils as part of a study by Daughtry, McMurtrey, Kim, and Chappelle (1996). The spectral diversity represented by these soils spans the range of reflectance encountered over the vast majority of midlatitude soils. The topsoil samples were first dried and the spectral reflectance measured. After the spectra of air-dried samples were acquired, the samples were thoroughly wetted with water and allowed to drain, and a second set of spectra was acquired. The range of spectral reflectances associated with each soil type is shown in Fig. 1. Whereas the overall shape of the spectral reflectance curve for a particular soil seems to be unaffected, the soil moisture content is governing the magnitude of the soil spectral reflectance. Each soil type was thus used as background in simulations where only LAI was varied to investigate the relative importance of soil background. The names and acronyms for the soils used in this study are summarized in Table 2.

### 2.3. Atmospheric effects

When satellite data are utilized to derive spectral reflectance for calculation of VIs, one has to consider their sensitivity to the absorption and scattering effects of the atmosphere. Both of these effects influence the extraterrestrial spectrum by modifying the spectral energy passing through the atmosphere, and so erroneous assumptions about the composition of the atmosphere at the time of data acquisition can have a significant impact on some VIs (Huete & Jackson, 1988; Slater & Jackson, 1982).

Several gases contribute to the overall atmospheric absorption of radiation in the solar spectrum. However, only the atmospheric gases oxygen ($O_2$), water vapor ($H_2O$), and ozone ($O_3$) are of interest in relation to this study because these gases exhibit absorption features within the VIS–NIR range (Vermote, Tanre, Deuze, Herman, & Morcrette, 1996). The $H_2O$ contribution mainly affects wavelengths greater than 700 nm. $O_3$ is a significant absorber between 550 and 650 nm, and the influence of $O_2$ is limited to a very strong but narrow band around 700 nm. Whereas the concentration of $O_2$ can be assumed constant at standard temperature and pressure (STP), $H_2O$ and $O_3$ concentrations normally depend on time of year and location.

Atmospheric scattering of direct solar radiation is usually described in terms of Maxwell's electromagnetic wave equation assuming that all scatterers are spheres. The scattering

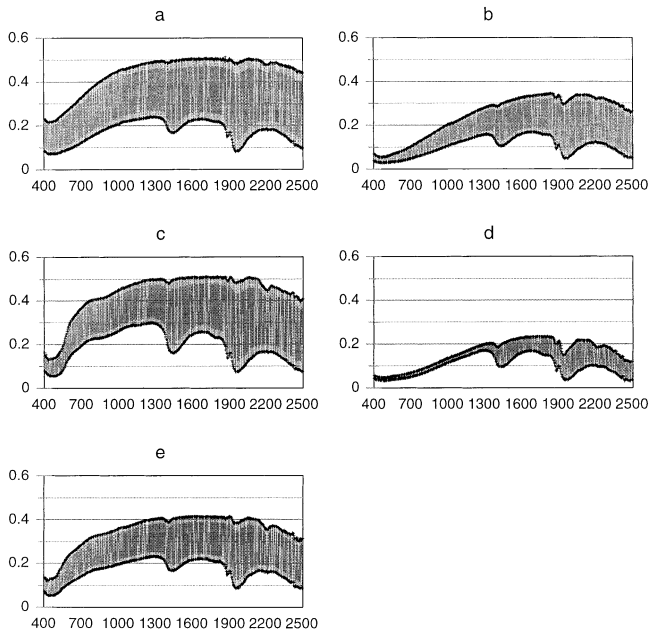


Fig. 1. Spectral reflectance of five spectrally distinct topsoils. Dry soil reflectance is represented by the top curve, and wet soil reflectance is represented by the bottom curve. A detailed description of each soil type can be found in Table 2.

Table 2
Names and acronyms for the soils used in this study

| Soil series | Classification | Moist soil color (Munsell) | Acronym |
|---|---|---|---|
| Othello | Fine-silty, mixed, active, mesic Typic Endoaquults | Dark greyish brown (2.5Y 4/2) | a |
| Barnes | Fine-loamy, mixed, superactive, frigid Calcic Hapludolls | Black (10YR 2/1) | b |
| Cecil | Fine, kaolinitic, thermic Typic Kanhapludults | Dark grayish brown (10YR 4/2) | c |
| Houston | Very-fine, smectitic, thermic Oxyaquic Hapluderts | Very dark gray (5Y 3/1) | d |
| Portneuf | Coarse-silty, mixed, superactive, mesic Durinodic Xeric Haplocalcids | Pale brown (10YR 6/3) | e |

caused by air molecules (Raleigh scattering) is a function of optical air mass and can therefore also be assumed constant at STP. However, the scattering caused by aerosols (Mie scattering) depends on the atmospheric turbidity or aerosol optical thickness as well as the form, size, distribution, and nature of the aerosols. The aerosol optical thickness ($\tau^A$) is a function of wavelength but is normally presented as the value at 550 nm ($\tau_{550}$), or estimated from synoptic measurements of horizontal visibility. The form and size and nature of aerosols can be described by grouping the aerosols into classes, i.e. Dust-like, Oceanic, Water-soluble, and Soot. The distribution can then be described by assigning an appropriate fraction to each class, so that the fractions sum up to unity.

The Second Simulation of the Satellite Signal in the Solar Spectrum (6S) model (Vermote et al., 1996) was used to investigate the effect of the atmosphere on the selected range of VIs. This model considers gaseous absorption as well as Rayleigh and Mie scattering including the interaction between these effects.

A look-up table relating ground reflectance to top-of-atmosphere (TOA) apparent spectral reflectance for each spectral band was created using the 6S model. The parameters used to simulate the canopy reflectances that were converted to TOA apparent reflectance are listed in Table 2 (Database 2 — Atmospheric effects). The atmospheric parameters used for the conversion were those of a standard midlatitude summer atmosphere ($H_2O = 2.93$ g/cm$^2$, $O_3 = 319$ DU[1]; McClatchey, Fenn, Selby, Volz, & Garing, 1971) and a continental aerosol mixture model where $\tau_{550} = 0.3$. The relationship between ground and TOA reflectance proved to be slightly curvilinear, allowing TOA apparent reflectance to be calculated directly from the look-up table using linear interpolation.

The TOA apparent spectral reflectances were then atmospherically corrected using 6S in forward mode to obtain ground reflectance for nine different combinations of atmospheric water vapor and visibility. Since $O_3$ concentration tends to be a function of latitude and season it was set constant to the model value for a midlatitude summer atmosphere ($O_3 = 319$ DU). Atmospheric $H_2O$ was set to 1.5, 2.93, and 4.5 g/cm$^2$ representing a normal range for midlatitude summer environments. Sunphotometer measurements obtained as part of the AERONET initiative (Holben et al., 1998) reveal a very wide range of aerosol optical thicknesses in a mixed urban and metropolitan area such as the eastern shore of the United States. Based on these records the aerosol optical thicknesses ($\tau_{550}$) for the simulations was set to 0.05 (clean), 0.3 (turbid), and 1.0 (very turbid). The aerosol model used was "continental" for the clean and turbid atmosphere, and "urban" for the very turbid atmosphere. Ground reflectance was then calculated for all combinations of $H_2O$ and $\tau_{550}$ based on the TOA apparent reflectance calculated from the simulated canopy reflectances.

## 3. Calculation of VIs

Most commonly used VIs are based on discrete Red and NIR bands, because vegetation exhibits unique reflectance properties in these bands. The early indices are generally divided into *ratio* indices and *orthogonal* indices depending upon their nature. Whereas ratio indices are calculated independently of soil reflectance properties, the orthogonal indices refer to a base line specific to the soil background. This soil line is normally defined by the coefficients *a* and *b* giving the slope and intercept as determined by linear regression of the soil reflectance in the Red–NIR spectral space. More recently, indices have emerged that can be considered *hybrid* versions of the classic ratio and orthogonal indices. Many VIs have been proposed over the past 30 years. In this study, seven of the most common VIs were selected for comparison with *hyperspectral* indices including one new index based on three discrete bands, i.e. Green, Red, and NIR bands.

All VIs were calculated from the simulated spectral data. The spectral data were simulated as adjacent 5 nm bands, and then resampled to 10 nm bands using a cubic spline function (Press, Flannery, Teukolsky, & Vetterling, 1989). Broadband ratio and orthogonal-based indices were calculated by spectral resampling of the 10 nm data using the Landsat TM5 filter functions (BSC, 1999). Narrowband versions of the selected VIs were calculated from the 670 (Red) and 800 nm (NIR) spectral bands.

### 3.1. Ratio VIs

Perhaps the best known of the classic VIs are the ratio vegetation index (RVI; Pearson & Miller, 1972) and the normalized difference vegetation index (NDVI; Rouse, Haas, Schell, Deering, & Harlan, 1974) that are based on

[1] Concentration of atmospheric gases is normally presented in Dobson Units (DU), where 1 DU is defined as 0.01 mm thickness at STP.

the reflectance in the Red and NIR part of the spectrum. RVI is the slope of the line that joins the origin and the vegetation point in Red–NIR space (Eq. (2)):

$$\mathrm{RVI} = \frac{\mathrm{NIR}}{\mathrm{Red}} = \tan(\theta_V) \tag{2}$$

where $\theta_V$ is the angle between this line and the abscissa. NDVI is also angularly defined and linked to the RVI (Eq. (3)):

$$\mathrm{NDVI} = \frac{\mathrm{NIR} - \mathrm{Red}}{\mathrm{NIR} + \mathrm{Red}} = \tan(\theta_V - \pi/4). \tag{3}$$

In general, these indices tend to enhance the contrast between soil and vegetation while minimizing the effects of illumination conditions (Baret & Guyot, 1991). However, they have been shown to be sensitive to soil brightness effects (Baret, Guyot, & Major, 1989; Huete, 1989; Roujean & Breon, 1995), especially at low vegetation cover (Fig. 2).

### 3.2. Orthogonal VIs

The second broad category of classic VIs are orthogonal transformations. These indices are distinct from the ratio-based indices in that the greenness isolines in the Red–NIR space do not converge in the origin, but instead remain parallel to the principal axis of soil spectral variation (Fig. 2). The perpendicular vegetation index (PVI; Richardson & Wiegand, 1977) represents the orthogonal distance between a point corresponding to canopy reflectance distance and the soil line in Red–NIR space (Eq. (4)):

$$\mathrm{PVI} = \frac{1}{\sqrt{a^2+1}}(\mathrm{NIR} - a \times \mathrm{Red} - b). \tag{4}$$

A simpler index related to PVI is the weighted difference vegetation index (WDVI; Clevers, 1989; Eq. (5)):

$$\mathrm{WDVI} = \mathrm{NIR} - a \times \mathrm{Red}. \tag{5}$$

However, as shown by Baret and Guyot (1991) and others, WDVI is functionally equivalent to PVI and was therefore omitted from the analysis. PVI simplifies to the difference vegetation index (DVI; Jordan, 1969) when the soil line parameters are $a=1$ and $b=0$. DVI is calculated simply as the difference between the NIR and the Red band (Eq. (6)):

$$\mathrm{DVI} = \mathrm{NIR} - \mathrm{Red}. \tag{6}$$

Unlike the angular indices (RVI and NDVI), PVI and DVI perform relatively well at low LAI values, i.e. relatively sparse vegetation cover, but they become more sensitive to soil background reflectance as LAI increases (Fig. 2).

### 3.3. Hybrid VIs

Soil-adjusted vegetation indices (SAVIs) were developed to account for changes of the optical properties of the background in an attempt to align the VI isolines with the greenness isolines (usually expressed in terms of LAI) over the entire dynamic range of the greenness measure. Huete (1988) proposed the first soil-adjusted vegetation index (SAVI), which includes a soil-adjustment factor ($L$) to account for first-order soil background variations (Eq. (7)).

$$\mathrm{SAVI} = \frac{\mathrm{NIR} - \mathrm{Red}}{\mathrm{NIR} + \mathrm{Red} + L}(1+L). \tag{7}$$

Huete (1988) found the optimal value of $L$ to vary with vegetation density, so he used a constant as optimization of $L$ would require prior knowledge of vegetation amounts. SAVI is an exact solution for bare soil only when the soil line parameters are $a=1$ and $b=0$. Baret et al. (1989) argued that a VI should be adjusted on specific soil line characteristics in order to be error-free at low LAI values. To achieve this goal they proposed the transformed SAVI (TSAVI; Eq. (8)). This index represents the angle between the soil line and the vegetation point in Red–NIR spectral space (Fig. 2).

$$\mathrm{TSAVI} = \frac{a(\mathrm{NIR} - a \times \mathrm{Red} - b)}{a \times \mathrm{NIR} + \mathrm{Red} - a \times b}. \tag{8}$$

Baret and Guyot (1991) later presented an improved version of TSAVI (in this paper referred to as the adjusted TSAVI [ATSAVI; Eq. (9)]) where the point of intersection of the vegetation isolines has been shifted into the third quadrant of the Red–NIR spectral space.

$$\mathrm{ATSAVI} = \frac{a(\mathrm{NIR} - a \times \mathrm{Red} - b)}{a \times \mathrm{NIR} + \mathrm{Red} - a \times b + X(1+a^2)}. \tag{9}$$

$X$ is an adjustment factor, which is set to minimize background effects ($X=0.08$ in the original paper by Baret and Guyot, 1991). Thus, the improvement of both TSAVI and ATSAVI over SAVI was to consider the actual gain ($a$) and intercept ($b$) values of the soil line rather than assuming them to be 1 and 0, respectively. Major, Baret, & Guyot (1990) used a simple canopy reflectance model to show that canopy NIR reflectance can be expressed as a linear function of canopy red reflectance. Based on this finding, they obtained a second version of the SAVI (SAVI2) that models the vegetation isoline behavior by using the ratio $b/a$ as the soil-adjustment factor (Eq. (10)).

$$\mathrm{SAVI2} = \frac{\mathrm{NIR}}{\mathrm{Red} + b/a}. \tag{10}$$

Qi, Chehbouni, Huete, Kerr, & Sorooshian (1994) proposed the second modified SAVI (MSAVI2), which replaces the soil-adjustment factor ($L$) of SAVI with a self-adjusting $L$ (Eq. (11)). The $L$ factor does not appear in the final mathematical formulation of MSAVI2, although an iterative $L$-function based on the product

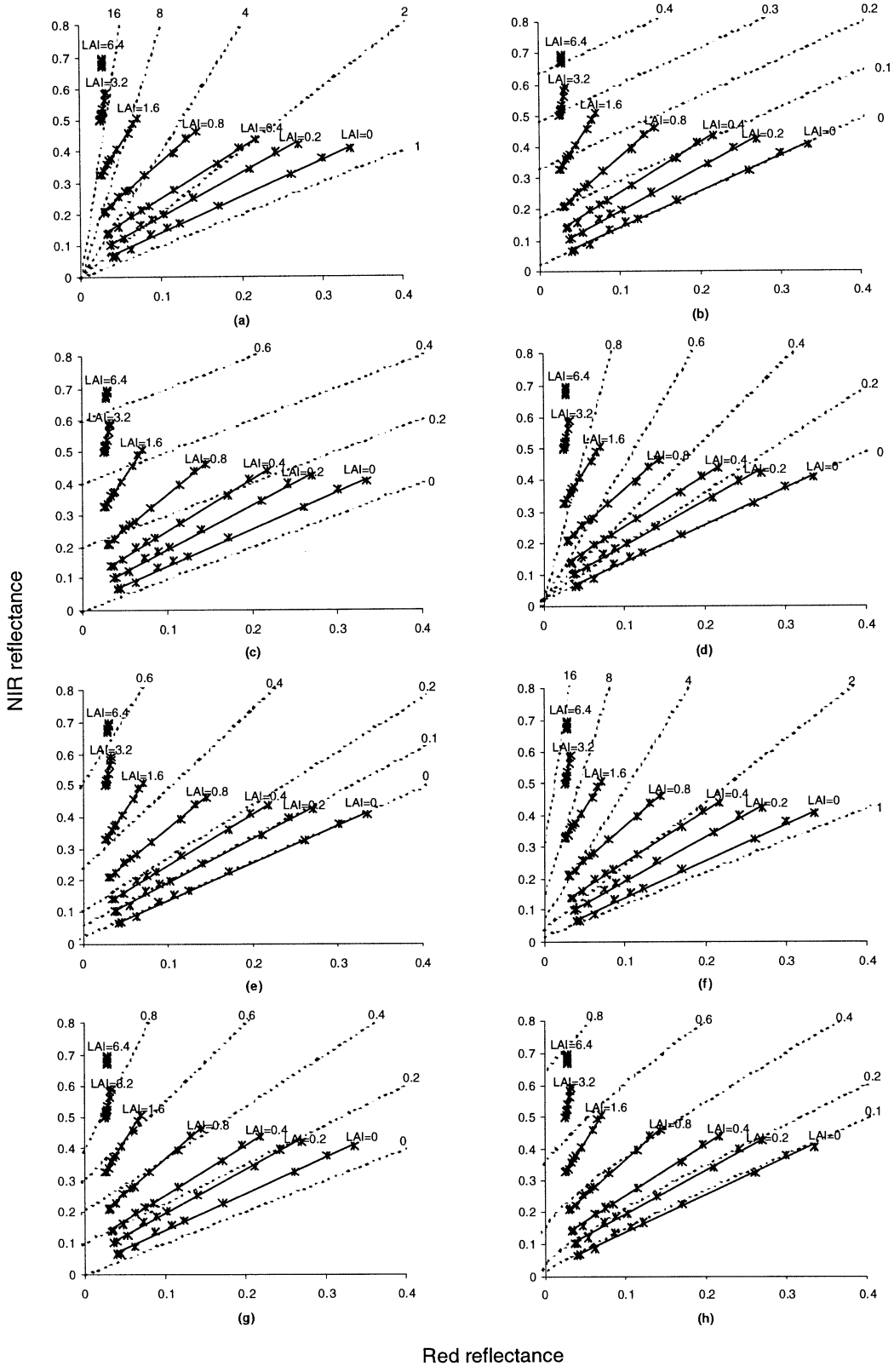


Fig. 2. The influence of soil background reflectance. The relationship between NIR and red reflectance for green LAI values (*) of 0, 0.2, 0.4, 0.8, 1.6, 3.2, and 6.4 is shown for different soil backgrounds. Red and NIR canopy reflectances were obtained from the "Background effects" database (Database 2, Table 1). GLAI isolines (solid lines) are shown together with VI isolines (broken lines) for (a) the angular indices (RVI and NDVI), (b) PVI, (c) DVI, (d) TSAVI, (e) ATASI, (f) SAVI2, (g) MSAVI2, and (h) RDVI. Parallel GLAI and VI isolines indicate that the VI is insensitive to soil background reflectance. The soil line parameters (GLAI = 0) are $a = 1.165$ and $b = 0.02288$.

of NDVI and WDVI was used in the derivation of the MSAVI2.

$$\text{MSAVI2} = \frac{1}{2}\left[2(\text{NIR}+1) - \sqrt{(2\text{NIR}+)^2 - 8(\text{NIR}-\text{Red})}\right]. \quad (11)$$

A relatively new index proposed by Roujean and Breon (1995), is the renormalized difference vegetation index (RDVI; Eq. (12)). This index is a hybrid between DVI and NDVI, and is supposed to combine the advantages of DVI and NDVI for low and high vegetation coverages, respectively (Fig. 2).

$$\text{RDVI} = \sqrt{\text{NDVI} \times \text{DVI}}. \quad (12)$$

### 3.4. New VIs based on two or three discrete bands

Three indices including a band in the green part of the spectrum were calculated. Kim, Daughtry, Chappelle, and McMurtrey (1994) found the ratio of 550 and 700 nm reflectance to be constant at the leaf level regardless of the differences in chlorophyll concentrations, and defined a chlorophyll absorption ratio index (CARI) based on this relationship and the chlorophyll absorption band at 670 nm (Eq. (13)).

$$\text{CARI} = \text{CAR}\frac{\text{R700}}{\text{R670}} \quad (13)$$

where CAR is the distance from the base line spanned by the green reflectance peak (R550) and the reflectance at 700 nm (R700). $\text{CAR} = |(a \times 670 + \text{R670} + b)|/(a^2+1)^{0.5}$, $a = (\text{R700} - \text{R550})/150$ and $b = \text{R550} - (a \times 550)$.

Gitelson, Merzlyak, & Lichtenthaler (1996), and Lichtenthaler et al. (1996) explored this idea and found strong correlation between leaf chlorophyll content and the reflectance ratios, R750/R700 and R750/R550.

A new VI denoted "triangular vegetation index" (TVI) was developed as part of this study. The general idea behind this index is to describe the radiative energy absorbed by the pigments as a function of the relative difference between red and NIR reflectance in conjunction with the magnitude of reflectance in the green region, where the light absorption by chlorophylls is relatively insignificant (Hall & Rao, 1987). The index is calculated as the area of the triangle defined by the green peak, the chlorophyll absorption minimum, and the NIR shoulder in spectral space. It is based on the fact that both chlorophyll absorption causing a decrease of red reflectance and leaf tissue abundance causing increased NIR reflectance will increase the total area of the triangle. The TVI index is thus defined as the area spanned by the triangle ABC with the coordinates given in spectral space (Eq. (14)):

$$\text{TVI} = 0.5|\det(AB, AC)| = 0.5(120(R_{\text{NIR}} - R_{\text{Green}}) - 200(R_{\text{Red}} - R_{\text{Green}})) \quad (14)$$

where $A = (550\text{ nm}, R_{\text{Green}})$, $B = (670\text{ nm}, R_{\text{Red}})$, and $C = (750\text{ nm}, R_{\text{NIR}})$.

### 3.5. Hyperspectral VIs

The characteristic red edge reflectance pattern of vegetation has been the subject of many studies (Collins, 1978; Gilabert et al., 1996; Gitelson et al., 1996; Horler, Dockray, & Barber, 1983), all of which have shown the observed blue-shift and red-shift of the red edge inflection point (REIP) to be related to plant growth conditions. REIP can be defined as the wavelength around 720 nm at which the first derivative of the spectral reflectance curve reaches its maximum value. REIP shifts toward shorter wavelengths (blue-shift) are associated with a decrease in green vegetation density, and REIP shifts toward longer wavelengths (red-shift) are likewise associated with an increase in green plant material.

#### 3.5.1. Parameterizing the red edge

The increase in vegetative chlorophyll-*a* concentration during the growth cycle has been shown to cause a red-shift of the inflection point (Horler, Dockray, & Barber, 1983; Horler, Dockray, Barber, & Barringer, 1983). Collins (1978) argues that this phenomenon is caused by polymer forms of chlorophyll adding closely spaced absorption bands to the far red shoulder of the main chlorophyll-*a* band. At the onset of senescence, the mesophyll structures in the plant tissue (effective near infrared reflectors) begin to collapse. Meanwhile, leaf chlorophyll decreases causing red reflectance to increase. These combined effects cause a blue-shift of REIP. Different techniques have been adopted to parameterize this spectral shift. In the present study, three different methods to derive the REIP were applied. Two measures that depend on the shape of the red edge, including the red and part of the NIR spectrum, were also tested.

Miller, Hare, and Wu (1990) used an inverted Gaussian model to describe the variation of reflectance as a function of wavelength, $R(\lambda)$. This approach has the advantage that it has a built-in smoothing of the red edge spectral reflectance and has been used by several authors (Bonham-Carter, 1988; Broge, Hvidberg, Hansen, Andersen, & Nielsen, 1997).

$$R(\lambda) = R_S - (R_S - R_0)\exp - \left[\frac{(\lambda - \lambda_0)^2}{2\sigma^2}\right]. \quad (15)$$

where $R_S$ is the "shoulder" reflectance at the NIR plateau, usually at 780–800 nm; $R_0$ is the minimum reflectance in the chlorophyll trough at approximately 670 nm; $\lambda_0$ is the wavelength of this minimum. $\sigma$ is the Gaussian shape parameter, such that $\text{REIP}_{\text{Gaus}} = \lambda_0 + \sigma$ is the inflection point of the red edge curve. The function is fitted to the measured reflection data, $R'(\lambda)$, by adjusting the values of $R_S$, $R_0$, $\lambda_0$

and σ, thus minimizing the root mean square error (RMSE) according to Eq. (16):

$$\mathrm{RMSE} = \sqrt{\frac{\sum_{i=1}^{N}[R(\lambda_i) - R'(\lambda_i)]^2}{N}} \tag{16}$$

where $N$ denotes the number of bands in the red edge wavelength interval ($N=16$ with 10 nm spectral resolution).

A similar way of determining REIP is fitting a higher order polynomial to the reflectance data in the red edge spectral range. A high-order polynomial will capture potential asymmetry of the red edge, whereas the inverted Gaussian model will average out such asymmetry. In this study, a sixth-order polynomial (Eq. (17)) was applied to derive the inflection point.

$$R(\lambda) = c_0 + c_1\lambda + c_2\lambda^2 + c_3\lambda^3 + c_4\lambda^4 + c_5\lambda^5 + c_6\lambda^6. \tag{17}$$

The VI denoted $\mathrm{REIP_{Poly}}$ was determined by identifying the roots of the second derivative of the polynomial ($R''(\lambda)=0$), adopting the root where λ was closer to 720 nm.

Recently, Dawson and Curran (1998) proposed a new way to determine REIP. They applied a technique known as Lagrangian interpolation (Press et al., 1989), which is applied to the first-derivative transformation of the reflectance spectrum. The technique fits a second-order polynomial curve to three bands, from which the REIP is determined. This approach was adopted as the third and last method of determining the REIP of the narrowband data.

Elvidge and Chen (1995) calculated the first and second derivatives of the spectral reflectance data and integrated the absolute derivative values over the spectral region from 626 to 795 nm, denoting these indices 1DZ_DGVI and 2DZ_DGVI. They also integrated the first derivative spectra with respect to the local baseline (1DL_DGVI). The performance of the latter two indices was shown to be practically identical, and thus only 1DZ_DGVI and 2DZ_DGVI were calculated in this study (Eqs. (18) and (19)):

$$\mathrm{1DZ\_DGVI} = \sum_{\lambda_1}^{\lambda_n} |\rho'(\lambda_i)|\Delta\lambda_i, \tag{18}$$

$$\mathrm{2DZ\_DGVI} = \sum_{\lambda_1}^{\lambda_n} |\rho''(\lambda_i)|\Delta\lambda_i. \tag{19}$$

*3.5.2. Indices based on spectral continuum measures*

An alternative way of utilizing hyperspectral reflectance data is to calculate the spectral continuum in which the analysis is based on the shape and area of the troughs spanned by the spectral continuum. This approach has been developed recently for airborne or satellite hyperspectral imaging instruments and is mostly used by geologists looking for distinct narrow absorption features in the spectra, i.e. physical fingerprints of minerals (Ben-dor & Kruse, 1995; Kruse, 1988). It can be used to identify and quantify any material that exhibits a discrete absorption feature such as chlorophylls in live vegetation. In this study, the area spanned by the chlorophyll absorption continuum ($\sim$550 to $\sim$730 nm) and the spectral reflectance curve was calculated and denoted the chlorophyll absorption continuum index (CACI; Eq. (20)).

$$\mathrm{CACI} = \sum_{\lambda_i}^{\lambda_n} (\rho_i^c - \rho_i)\Delta\lambda_i, \quad \text{where } \rho_i^c = \rho_1 + i\frac{\mathrm{d}\rho^c}{\mathrm{d}\lambda}\Delta\lambda_i. \tag{20}$$

This index is similar to the TVI index in the sense that both indices represent the area spanned by the spectral reflectance between the green peak and the NIR plateau. However, all the spectral bands between the green peak and the NIR shoulder are utilized when calculating CACI.

Continuum removal is taking this approach one step further. Continuum removal is a means of normalizing reflectance spectra to allow comparison of individual absorption features from a common baseline. The continuum is a convex hull fit over the top of a spectrum utilizing straight-line segments that connect local spectral maxima. The first and last spectral data values are on the hull and therefore the first and last bands in the continuum-removed data will be equal to 1.0. The continuum was removed by dividing it into the actual spectrum. The resulting image spectra are equal to 1.0 where the continuum and the spectra match and less than 1.0 where absorption features occur. The continuum removed chlorophyll absorption index (CRCAI; Eq. (21)) was defined as the area spanned by the continuum-removed spectra and the continuum, i.e. the $y=1$ line after continuum removal.

$$\mathrm{CRCAI} = \sum_{\lambda_1}^{\lambda_n} \frac{\rho_i^c - \rho_i}{\rho_i^c}\Delta\lambda_i, \quad \text{where } \rho_i^c = \rho_1 + i\frac{d\rho^c}{d\lambda}\Delta\lambda_i. \tag{21}$$

Another measure of the continuum-normalized spectrum is the maximum depth of the chlorophyll absorption trough. This measure is herein referred to as the continuum-removed chlorophyll well depth (CRCWD), which is a value between 0 and 1. It is thus directly comparable with many traditional VIs such as NDVI and TSAVI.

## 4. Relating LAI and CCD to VIs

Because most VIs, including the REIP, approach a saturation level with increasing green biomass, they can be fitted to an exponential function. A modified version of Beer's law has been suggested (Baret & Guyot, 1991; Wiegand et al., 1992) to describe the relationship between a VI and LAI or APAR. This model was adopted in this study to quantify the

Table 3

| Index | $VI_G$ | $VI_{INF}$ | $K_{VI}$ | RMSE | $RMSE_{NORM}$ | Adj. $R^2$ |
|---|---|---|---|---|---|---|
| (a) LAI coefficients for Eq. (22) — Database 1 (Canopy effects) | | | | | | |
| $REIP_{Poly}$ | 715.9508 | 737.2274 | 0.2734 | 6.9128 | 0.3249 | 0.5041 |
| $REIP_{Gaus}$ | 711.9259 | 723.8883 | 0.2013 | 4.5650 | 0.3816 | 0.3886 |
| $REIP_{Lagr}$ | 713.3438 | 742.9460 | 0.3783 | 8.6280 | 0.2915 | 0.5807 |
| DGVI_DZ1 | 0.0604 | 0.7453 | 0.3138 | 0.0781 | 0.1141 | 0.8964 |
| DGVI_DZ2 | 0.0009 | 0.0420 | 0.2323 | 0.0047 | 0.1155 | 0.8824 |
| CACI | 1.5588 | 57.7345 | 0.3071 | 5.9193 | 0.1054 | 0.9097 |
| CRCAI | 13.4624 | 139.0426 | 0.9933 | 13.0054 | 0.1036 | 0.9122 |
| CRCWD | 7.9383 | 92.6784 | 1.4344 | 5.5845 | 0.0659 | 0.9570 |
| CARI | − 0.0105 | 13.1909 | 0.4931 | 6.5629 | 0.4971 | 0.3291 |
| R750R700 | 0.6746 | 10.1558 | 0.4045 | 2.5898 | 0.2731 | 0.6147 |
| R750R550 | 1.4163 | 9.5608 | 0.4277 | 2.4226 | 0.2974 | 0.5755 |
| N_RVI | − 0.3787 | 28.0060 | 0.3176 | 5.6929 | 0.2006 | 0.7373 |
| N_NDVI | 0.1734 | 0.9108 | 1.1518 | 0.0514 | 0.0697 | 0.9561 |
| N_TVI | 1.2940 | 40.0103 | 0.3895 | 4.9925 | 0.1290 | 0.8768 |
| N_DVI | 0.0540 | 0.7203 | 0.3218 | 0.0756 | 0.1135 | 0.8979 |
| N_RDVI | 0.1138 | 0.7909 | 0.5125 | 0.0609 | 0.0900 | 0.9377 |
| N_MSAVI2 | 0.5663 | 1.3906 | 0.5437 | 0.0719 | 0.0872 | 0.9412 |
| N_PVI | 0.0076 | 0.4535 | 0.3279 | 0.0498 | 0.1118 | 0.9012 |
| N_TSAVI | 0.0158 | 0.9043 | 1.2012 | 0.0614 | 0.0691 | 0.9563 |
| N_SAVI2 | 0.5877 | 13.7091 | 0.3256 | 1.5678 | 0.1195 | 0.8885 |
| N_ATSAVI | 0.0225 | 0.8070 | 0.7487 | 0.0601 | 0.0766 | 0.9529 |
| B_RVI | 0.2746 | 22.7927 | 0.3283 | 5.1316 | 0.2279 | 0.6869 |
| B_NDVI | 0.2205 | 0.8904 | 1.0985 | 0.0541 | 0.0808 | 0.9429 |
| B_TVI | 3.4193 | 45.5142 | 0.3217 | 4.7534 | 0.1129 | 0.8989 |
| B_DVI | 0.0672 | 0.7280 | 0.3088 | 0.0744 | 0.1126 | 0.8984 |
| B_RDVI | 0.1376 | 0.7869 | 0.4859 | 0.0597 | 0.0920 | 0.9348 |
| B_MSA2VI | 0.5911 | 1.3709 | 0.5320 | 0.0711 | 0.0911 | 0.9362 |
| B_PVI | 0.0164 | 0.4578 | 0.3144 | 0.0490 | 0.1109 | 0.9015 |
| B_TSAVI | 0.0785 | 0.8827 | 1.1423 | 0.0628 | 0.0781 | 0.9457 |
| B_SAVI2 | 0.8260 | 12.3091 | 0.3276 | 1.6770 | 0.1460 | 0.8423 |
| B_ATSAVI | 0.0597 | 0.7920 | 0.7162 | 0.0602 | 0.0822 | 0.9465 |
| (b) LAI coefficients for Eq. (22) — Database 2 (Background effects) | | | | | | |
| $REIP_{Poly}$ | 718.1625 | 738.0320 | 0.2999 | 0.5937 | 0.0299 | 0.9919 |
| $REIP_{Gaus}$ | 710.8325 | 723.5917 | 0.3064 | 1.1873 | 0.0931 | 0.9269 |
| $REIP_{Lagr}$ | 716.7261 | 744.0661 | 0.4662 | 1.5967 | 0.0584 | 0.9722 |
| DGVI_DZ1 | 0.0659 | 0.7505 | 0.3407 | 0.0313 | 0.0457 | 0.9819 |
| DGVI_DZ2 | 0.0011 | 0.0442 | 0.2314 | 0.0015 | 0.0344 | 0.9881 |
| CACI | 0.7603 | 58.5364 | 0.3422 | 1.9165 | 0.0332 | 0.9904 |
| CRCAI | 7.1589 | 143.0635 | 1.0951 | 9.3923 | 0.0691 | 0.9569 |
| CRCWD | 5.7640 | 94.0638 | 1.5243 | 6.1480 | 0.0696 | 0.9500 |
| CARI | − 0.0279 | 10.9919 | 0.4726 | 0.2573 | 0.0233 | 0.9955 |
| R750R700 | 0.5534 | 10.0476 | 0.4819 | 0.3929 | 0.0414 | 0.9859 |
| R750R550 | 1.4541 | 9.4278 | 0.5153 | 0.3002 | 0.0377 | 0.9883 |
| N_RVI | − 1.1020 | 29.5150 | 0.3806 | 1.6613 | 0.0543 | 0.9752 |
| N_NDVI | 0.1503 | 0.9282 | 1.2467 | 0.0512 | 0.0658 | 0.9589 |
| N_TVI | 0.9274 | 40.2132 | 0.4307 | 1.4258 | 0.0363 | 0.9890 |
| N_DVI | 0.0584 | 0.7293 | 0.3515 | 0.0305 | 0.0454 | 0.9822 |
| N_RDVI | 0.1016 | 0.8036 | 0.5771 | 0.0189 | 0.0269 | 0.9940 |
| N_MSAVI2 | 0.5442 | 1.4138 | 0.6239 | 0.0204 | 0.0235 | 0.9954 |
| N_PVI | 0.0068 | 0.4595 | 0.3620 | 0.0181 | 0.0401 | 0.9862 |
| N_TSAVI | − 0.0252 | 0.9223 | 1.3380 | 0.0420 | 0.0443 | 0.9804 |
| N_SAVI2 | 0.2462 | 14.7820 | 0.3636 | 0.4274 | 0.0294 | 0.9925 |
| N_ATSAVI | − 0.0105 | 0.8263 | 0.8443 | 0.0132 | 0.0158 | 0.9978 |
| B_RVI | − 0.2763 | 23.5007 | 0.3955 | 1.1629 | 0.0489 | 0.9799 |
| B_NDVI | 0.1857 | 0.9113 | 1.1979 | 0.0522 | 0.0719 | 0.9520 |
| B_TVI | 2.9509 | 45.9251 | 0.3566 | 1.7516 | 0.0408 | 0.9857 |
| B_DVI | 0.0680 | 0.7380 | 0.3392 | 0.0312 | 0.0465 | 0.9812 |
| B_RDVI | 0.1192 | 0.8014 | 0.5529 | 0.0194 | 0.0285 | 0.9933 |
| B_MSA2VI | 0.5629 | 1.3955 | 0.6146 | 0.0206 | 0.0247 | 0.9949 |
| B_PVI | 0.0134 | 0.4646 | 0.3491 | 0.0186 | 0.0412 | 0.9853 |
| B_TSAVI | 0.0266 | 0.9047 | 1.2768 | 0.0435 | 0.0495 | 0.9761 |
| B_SAVI2 | 0.4853 | 13.1913 | 0.3706 | 0.3507 | 0.0276 | 0.9934 |
| B_ATSAVI | 0.0170 | 0.8139 | 0.8177 | 0.0149 | 0.0187 | 0.997 |
| (c) LAI coefficients for Eq. (22) — Database 3 (Atmospheric effects) | | | | | | |
| $REIP_{Poly}$ | 717.4049 | 738.2075 | 0.2959 | 4.8097 | 0.2312 | 0.6681 |
| $REIP_{Gaus}$ | 711.2736 | 724.1225 | 0.2836 | 2.7463 | 0.2137 | 0.6991 |
| $REIP_{Lagr}$ | 720.9583 | 745.5226 | 0.2862 | 5.9258 | 0.2412 | 0.6461 |
| DGVI_DZ1 | 0.0563 | 0.6691 | 0.3219 | 0.1204 | 0.1965 | 0.7414 |
| DGVI_DZ2 | 0.0037 | 0.0405 | 0.2177 | 0.0058 | 0.1581 | 0.7913 |
| CACI | 1.2044 | 50.8998 | 0.3142 | 9.6204 | 0.1936 | 0.7458 |
| CRCAI | 15.2997 | 140.9451 | 1.0547 | 10.7145 | 0.0853 | 0.9365 |
| CRCWD | 8.5133 | 92.8140 | 1.5308 | 5.2322 | 0.0621 | 0.9597 |
| CARI | − 0.6381 | 13.6956 | 0.4822 | 6.8612 | 0.4787 | 0.3341 |
| R750R700 | 0.5518 | 9.6191 | 0.4944 | 1.6315 | 0.1799 | 0.7859 |
| R750R550 | 1.4325 | 9.9761 | 0.5298 | 1.4815 | 0.1734 | 0.7985 |
| N_RVI | − 3.2190 | 38.9229 | 0.4281 | 18.1019 | 0.4295 | 0.3830 |
| N_NDVI | 0.1691 | 0.9143 | 1.2832 | 0.0569 | 0.0763 | 0.9448 |
| N_TVI | 0.9419 | 34.8280 | 0.3993 | 7.2481 | 0.2139 | 0.7171 |
| N_DVI | 0.0477 | 0.6406 | 0.3310 | 0.1173 | 0.1978 | 0.7402 |
| N_RDVI | 0.1075 | 0.7415 | 0.5437 | 0.1014 | 0.1599 | 0.8234 |
| N_MSAVI2 | 0.5512 | 1.3420 | 0.5752 | 0.1379 | 0.1744 | 0.7965 |
| N_PVI | 0.0047 | 0.4016 | 0.3378 | 0.0780 | 0.1967 | 0.7435 |
| N_TSAVI | − 0.0170 | 0.9063 | 1.3347 | 0.0724 | 0.0784 | 0.9409 |
| N_SAVI2 | 0.2425 | 14.6646 | 0.3697 | 3.9311 | 0.2726 | 0.6050 |
| N_ATSAVI | 0.0078 | 0.7805 | 0.7875 | 0.0992 | 0.1284 | 0.8750 |
| B_RVI | − 1.6192 | 30.3243 | 0.4388 | 11.7678 | 0.3684 | 0.4603 |
| B_NDVI | 0.2161 | 0.9065 | 1.2530 | 0.0526 | 0.0762 | 0.9455 |
| B_TVI | 2.8295 | 40.7737 | 0.3333 | 7.3343 | 0.1933 | 0.7495 |
| B_DVI | 0.0591 | 0.6553 | 0.3198 | 0.1153 | 0.1934 | 0.7471 |
| B_RDVI | 0.1300 | 0.7474 | 0.5209 | 0.0975 | 0.1580 | 0.8269 |
| B_MSA2VI | 0.5733 | 1.3395 | 0.5653 | 0.1281 | 0.1672 | 0.8099 |
| B_PVI | 0.0124 | 0.4110 | 0.3261 | 0.0766 | 0.1923 | 0.7503 |
| B_TSAVI | 0.0478 | 0.8983 | 1.3010 | 0.0667 | 0.0784 | 0.9416 |
| B_SAVI2 | 0.4753 | 13.6349 | 0.3755 | 3.3715 | 0.2562 | 0.6352 |
| B_ATSAVI | 0.0429 | 0.7792 | 0.7655 | 0.0934 | 0.1268 | 0.8783 |
| (d) CCD coefficients for Eq. (22) — Database 1 (Canopy effects) | | | | | | |
| $REIP_{Poly}$ | 714.7183 | 740.9323 | 0.4884 | 4.9656 | 0.1894 | 0.7441 |
| $REIP_{Gaus}$ | 711.0099 | 728.1105 | 0.3090 | 3.2364 | 0.1893 | 0.6927 |
| $REIP_{Lagr}$ | 710.3510 | 744.1798 | 0.9338 | 6.1158 | 0.1808 | 0.7893 |
| DGVI_DZ1 | 0.0666 | 0.6912 | 0.8554 | 0.1074 | 0.1720 | 0.8040 |
| DGVI_DZ2 | 0.0025 | 0.0461 | 0.3815 | 0.0039 | 0.0891 | 0.9208 |
| CACI | 2.5564 | 55.4691 | 0.7296 | 7.5343 | 0.1424 | 0.8537 |
| CRCAI | 19.3801 | 143.2575 | 1.7764 | 11.2330 | 0.0907 | 0.9345 |
| CRCWD | 11.7055 | 93.0564 | 2.9427 | 7.9376 | 0.0976 | 0.9131 |
| CARI | − 1.5639 | 10.6310 | 3.7128 | 7.1363 | 0.5852 | 0.2068 |
| R750R700 | 1.1265 | 13.3636 | 0.4104 | 1.7362 | 0.1419 | 0.8268 |
| R750R550 | 1.7795 | 12.5244 | 0.4142 | 1.6354 | 0.1522 | 0.8065 |
| N_RVI | 0.6465 | 32.7352 | 0.4576 | 4.3533 | 0.1357 | 0.8464 |
| N_NDVI | 0.1941 | 0.9159 | 2.4193 | 0.0646 | 0.0896 | 0.9307 |
| N_TVI | 0.9808 | 36.5406 | 1.2018 | 6.8345 | 0.1922 | 0.7692 |
| N_DVI | 0.0612 | 0.6789 | 0.8334 | 0.0995 | 0.1611 | 0.8234 |
| N_RDVI | 0.1141 | 0.7712 | 1.2958 | 0.0810 | 0.1233 | 0.8896 |
| N_MSAVI2 | 0.5751 | 1.3786 | 1.2806 | 0.0934 | 0.1163 | 0.9008 |
| N_PVI | 0.0122 | 0.4269 | 0.8463 | 0.0656 | 0.1581 | 0.8291 |
| N_TSAVI | 0.0420 | 0.9097 | 2.5243 | 0.0789 | 0.0909 | 0.9277 |
| N_SAVI2 | 0.9944 | 14.5370 | 0.5826 | 1.2622 | 0.0932 | 0.9277 |
| N_ATSAVI | 0.0283 | 0.8021 | 1.7470 | 0.0792 | 0.1024 | 0.9182 |
| B_RVI | 1.1751 | 28.6388 | 0.3995 | 3.5563 | 0.1295 | 0.8496 |
| B_NDVI | 0.2412 | 0.9006 | 2.1982 | 0.0550 | 0.0834 | 0.9411 |
| B_TVI | 3.8217 | 42.6207 | 0.8526 | 6.3892 | 0.1647 | 0.8173 |
| B_DVI | 0.0752 | 0.6901 | 0.7812 | 0.0957 | 0.1556 | 0.8319 |

(continued on next page)

Table 3 (*continued*)

| Index | $VI_G$ | $VI_{INF}$ | $K_{VI}$ | RMSE | $RMSE_{NORM}$ | Adj. $R^2$ |
|---|---|---|---|---|---|---|
| B_RDVI | 0.1397 | 0.7727 | 1.1832 | 0.0736 | 0.1162 | 0.9012 |
| B_MSA2VI | 0.6018 | 1.3683 | 1.1946 | 0.0824 | 0.1075 | 0.9142 |
| B_PVI | 0.0216 | 0.4340 | 0.7900 | 0.0627 | 0.1519 | 0.8387 |
| B_TSAVI | 0.1037 | 0.8934 | 2.3050 | 0.0667 | 0.0845 | 0.9388 |
| B_SAVI2 | 1.2272 | 13.7779 | 0.5075 | 1.0624 | 0.0846 | 0.9367 |
| B_ATSAVI | 0.0674 | 0.7936 | 1.5995 | 0.0686 | 0.0945 | 0.9306 |
| (e) CCD coefficients for Eq. (22) — Database 2 (Background effects) | | | | | | |
| $REIP_{Poly}$ | 718.1625 | 738.0320 | 0.5998 | 0.5937 | 0.0299 | 0.9919 |
| $REIP_{Gaus}$ | 710.8325 | 723.5917 | 0.6127 | 1.1873 | 0.0931 | 0.9269 |
| $REIP_{Lagr}$ | 716.7261 | 744.0662 | 0.9323 | 1.5967 | 0.0584 | 0.9722 |
| DGVI_DZ1 | 0.0659 | 0.7505 | 0.6813 | 0.0313 | 0.0457 | 0.9819 |
| DGVI_DZ2 | 0.0011 | 0.0442 | 0.4628 | 0.0015 | 0.0344 | 0.9881 |
| CACI | 0.7603 | 58.5364 | 0.6843 | 1.9165 | 0.0332 | 0.9904 |
| CRCAI | 7.1589 | 143.0635 | 2.1903 | 9.3923 | 0.0691 | 0.9569 |
| CRCWD | 5.7641 | 94.0638 | 3.0486 | 6.1480 | 0.0696 | 0.9500 |
| CARI | −0.0279 | 10.9919 | 0.9452 | 0.2573 | 0.0233 | 0.9955 |
| R750R700 | 0.5534 | 10.0476 | 0.9638 | 0.3929 | 0.0414 | 0.9859 |
| R750R550 | 1.4541 | 9.4278 | 1.0307 | 0.3002 | 0.0377 | 0.9883 |
| N_RVI | −1.1020 | 29.5150 | 0.7611 | 1.6613 | 0.0543 | 0.9752 |
| N_NDVI | 0.1503 | 0.9282 | 2.4933 | 0.0512 | 0.0658 | 0.9589 |
| N_TVI | 0.9274 | 40.2132 | 0.8615 | 1.4258 | 0.0363 | 0.9890 |
| N_DVI | 0.0584 | 0.7293 | 0.7030 | 0.0305 | 0.0454 | 0.9822 |
| N_RDVI | 0.1016 | 0.8036 | 1.1542 | 0.0189 | 0.0269 | 0.9940 |
| N_MSAVI2 | 0.5442 | 1.4138 | 1.2479 | 0.0204 | 0.0235 | 0.9954 |
| N_PVI | 0.0068 | 0.4595 | 0.7240 | 0.0181 | 0.0401 | 0.9862 |
| N_TSAVI | −0.0252 | 0.9223 | 2.6760 | 0.0420 | 0.0443 | 0.9804 |
| N_SAVI2 | 0.2462 | 14.7820 | 0.7272 | 0.4274 | 0.0294 | 0.9925 |
| N_ATSAVI | −0.0105 | 0.8263 | 1.6886 | 0.0132 | 0.0158 | 0.9978 |
| B_RVI | −0.2763 | 23.5007 | 0.7911 | 1.1629 | 0.0489 | 0.9799 |
| B_NDVI | 0.1857 | 0.9113 | 2.3958 | 0.0522 | 0.0719 | 0.9520 |
| B_TVI | 2.9509 | 45.9251 | 0.7131 | 1.7516 | 0.0408 | 0.9857 |
| B_DVI | 0.0680 | 0.7380 | 0.6783 | 0.0312 | 0.0465 | 0.9812 |
| B_RDVI | 0.1192 | 0.8014 | 1.1057 | 0.0194 | 0.0285 | 0.9933 |
| B_MSA2VI | 0.5629 | 1.3955 | 1.2293 | 0.0206 | 0.0247 | 0.9949 |
| B_PVI | 0.0134 | 0.4646 | 0.6983 | 0.0186 | 0.0412 | 0.9853 |
| B_TSAVI | 0.0266 | 0.9047 | 2.5536 | 0.0435 | 0.0495 | 0.9761 |
| B_SAVI2 | 0.4853 | 13.1913 | 0.7413 | 0.3507 | 0.0276 | 0.9934 |
| B_ATSAVI | 0.0170 | 0.8139 | 1.6355 | 0.0149 | 0.0187 | 0.997 |
| (f) CCD coefficients for Eq. (22) — Database 3 (Atmospheric effects) | | | | | | |
| $REIP_{Poly}$ | 717.4049 | 738.2075 | 0.5919 | 4.8097 | 0.2312 | 0.6681 |
| $REIP_{Gaus}$ | 711.2736 | 724.1225 | 0.5671 | 2.7463 | 0.2137 | 0.6991 |
| $REIP_{Lagr}$ | 720.9586 | 745.5233 | 0.5723 | 5.9258 | 0.2412 | 0.6461 |
| DGVI_DZ1 | 0.0563 | 0.6691 | 0.6438 | 0.1204 | 0.1965 | 0.7414 |
| DGVI_DZ2 | 0.0037 | 0.0405 | 0.4355 | 0.0058 | 0.1581 | 0.7913 |
| CACI | 1.2044 | 50.8998 | 0.6283 | 9.6204 | 0.1936 | 0.7458 |
| CRCAI | 15.2995 | 140.9451 | 2.1093 | 10.7145 | 0.0853 | 0.9365 |
| CRCWD | 8.5133 | 92.814 | 3.0616 | 5.2322 | 0.0621 | 0.9597 |
| CARI | −0.6382 | 13.6955 | 0.9644 | 6.8612 | 0.4787 | 0.3341 |
| R750R700 | 0.5517 | 9.6191 | 0.9887 | 1.6315 | 0.1799 | 0.7859 |
| R750R550 | 1.4325 | 9.9761 | 1.0596 | 1.4815 | 0.1734 | 0.7985 |
| N_RVI | −3.2176 | 38.9248 | 0.8561 | 18.1019 | 0.4295 | 0.383 |
| N_NDVI | 0.1691 | 0.9143 | 2.5663 | 0.0569 | 0.0763 | 0.9448 |
| N_TVI | 0.9419 | 34.828 | 0.7987 | 7.2481 | 0.2139 | 0.7171 |
| N_DVI | 0.0477 | 0.6406 | 0.662 | 0.1173 | 0.1978 | 0.7402 |
| N_RDVI | 0.1075 | 0.7415 | 1.0873 | 0.1014 | 0.1599 | 0.8234 |
| N_MSAVI2 | 0.5512 | 1.342 | 1.1504 | 0.1379 | 0.1744 | 0.7965 |
| N_PVI | 0.0047 | 0.4016 | 0.6756 | 0.078 | 0.1967 | 0.7435 |
| N_TSAVI | −0.017 | 0.9063 | 2.6694 | 0.0724 | 0.0784 | 0.9409 |
| N_SAVI2 | 0.2425 | 14.6646 | 0.7394 | 3.9311 | 0.2726 | 0.605 |
| N_ATSAVI | 0.0078 | 0.7805 | 1.5751 | 0.0992 | 0.1284 | 0.875 |
| B_RVI | −1.6194 | 30.324 | 0.8775 | 11.7678 | 0.3684 | 0.4603 |

Table 3 (*continued*)

| Index | $VI_G$ | $VI_{INF}$ | $K_{VI}$ | RMSE | $RMSE_{NORM}$ | Adj. $R^2$ |
|---|---|---|---|---|---|---|
| B_NDVI | 0.2161 | 0.9065 | 2.506 | 0.0526 | 0.0762 | 0.9455 |
| B_TVI | 2.8295 | 40.7737 | 0.6666 | 7.3343 | 0.1933 | 0.7495 |
| B_DVI | 0.0591 | 0.6553 | 0.6395 | 0.1153 | 0.1934 | 0.7471 |
| B_RDVI | 0.13 | 0.7474 | 1.0418 | 0.0975 | 0.158 | 0.8269 |
| B_MSA2VI | 0.5733 | 1.3395 | 1.1307 | 0.1281 | 0.1672 | 0.8099 |
| B_PVI | 0.0124 | 0.411 | 0.6521 | 0.0766 | 0.1923 | 0.7503 |
| B_TSAVI | 0.0478 | 0.8983 | 2.6021 | 0.0667 | 0.0784 | 0.9416 |
| B_SAVI2 | 0.4753 | 13.6349 | 0.751 | 3.3715 | 0.2562 | 0.6352 |
| B_ATSAVI | 0.0429 | 0.7792 | 1.5311 | 0.0934 | 0.1268 | 0.8783 |

sensitivity of the calculated indices to solar zenith angle, mean leaf tip angle, and background reflectance.

$$VI = VI_\infty + (VI_g - VI_\infty)\exp^{(-K_{VI}LAI)}. \quad (22)$$

The model assumes the canopy to be a homogenous substance of green plant material with an optical thickness given by LAI. The dynamic range of the VI is expressed as the difference between the bulk VI, $VI_\infty$, and the index value corresponding to bare soil conditions, $VI_g$. The $K_{VI}$ parameter is equivalent to the extinction coefficient in Beer's law and represents the relative increase in VI due to an elementary increase in the greenness measure (LAI or CCD). In this study, the model (Eq. (22)) was used to obtain relationships of the selected VIs with LAI and CCD, defining CCD as the product of leaf chlorophyll content ($Chl_{a+b}$ [μg/cm2]) and LAI.

$K_{VI}$ and $VI_\infty$ were obtained for different combinations of solar zenith angle ($\theta_s$), mean leaf tip angle, (MTA) and Chl $a+b$ (for LAI prediction only). $VI_g$ was obtained from soiltype $a$ (Table 1). The Marquardt nonlinear regression method (Marquardt, 1963) was used to fit the model (Eq. (22)) by the least squares method. VI($i$) and either LAI($i$) or CCD($i$) were used as input vectors, where $i$ denotes a specific combination of simulation input parameters. The RMSE and the adjusted coefficient of determination ($R^2$) were calculated along with the normalized RMSE given as $RMSE/(VI_\infty - VI_g)$. The modelled coefficients and the statistics associated with the fit are given in Table 3a–f. These statistics are all associated with the accuracy of the curve fit, but they do not provide any information about the prediction power of the VIs because of the nonlinear nature of the relationship between the VIs and the biophysical parameters. The prediction power is inversely related to the sensitivity to all parameters other than the one (in this study LAI or CCD) for which the VI serves as a predictor. To obtain this information, the shape of the exponential function relating the VIs and the biophysical parameters needs to be considered in conjunction with the associated variance.

## 5. Sensitivity analysis

The sensitivities of the VIs to external factors were analyzed using the relative equivalent noise approach

(REN) proposed by (Baret & Guyot, 1991). These authors used the local slope of the exponential function fitted to the data to calculate the standard deviation of the greenness estimate according to the equation:

$$\mathrm{REN}_{\mathrm{LAI}} = \frac{\sigma_{\mathrm{LAI}}}{\mathrm{LAI}} = \frac{\sigma_{\mathrm{VI}}}{\mathrm{LAI}} \left( \frac{\mathrm{d(VI)}}{\mathrm{d(LAI)}} \right)^{-1}. \quad (23)$$

The local slope (Eq. (24)) can be found by differentiation of Eq. (23):

$$\frac{\mathrm{d(VI)}}{\mathrm{d(LAI)}} = -\mathrm{K}_{\mathrm{VI}}(\mathrm{VI}_{\mathrm{g}} - VI_{\infty})\exp^{(-\mathrm{K}_{\mathrm{VI}}\mathrm{LAI})}. \quad (24)$$

The advantage of the REN measure is that it allows for a comparison of VIs for any value or interval of values of the independent variable (LAI or CCD), thus facilitating a unique method for intercomparison of the performance of the VIs.

## 6. Results and discussion

### 6.1. The REIP

REIP was determined in two fundamentally different ways. The polynomial fitting procedure (Eq. (17)) and the inverted Gaussian model (Eq. (15)) proposed by Bonham-Carter (1988) and Miller et al. (1990) both approximate the spectral shape of the red edge by fitting a function to the spectral data. This method has a built-in smoothing routine because REIP is determined by differentiation of these functions. The Lagrangian technique proposed by Dawson and Curran (1998) forces the interpolation curve through the given points, thus taking into account the curvature of the function. The drawback of this method is that it is more sensitive to the inherent spectral noise of the system.

The three methods were compared using the canopy effects data to calculate the frequency distribution of each of the three methods of REIP determination (Fig. 3). It is evident from Fig. 3 that results of REIP calculations are highly dependent upon the choice of methodology. The $\mathrm{REIP}_{\mathrm{Gaus}}$ data resemble a Gaussian distribution reflecting the exponential relationship between REIP and vegetation density because of the overrepresentation of low LAI values in the data set. $\mathrm{REIP}_{\mathrm{Poly}}$ shows a wider dynamic range and its distribution is slightly skewed to the right, suggesting higher sensitivity to low LAI values. It is further interesting to note that the three phases of REIP first described by Horler, Dockray, and Barber (1983) and later confirmed by Boochs, Kupfer, Dockter, & Kühbach (1997) and Gitelson et al. (1996) are clearly visible in the $\mathrm{REIP}_{\mathrm{Lagr}}$ data. These studies showed that two to four peaks can be identified in the second derivative reflectance spectra at both leaf and canopy level. Boochs et al. (1997) calculated spectral derivatives over the red edge region of differently managed field plots of sugar beet and wheat. They identified two or three dominant peaks in the first derivative spectra, as Horler et al. (1983) had done previously for various leaf species. Both of these authors maintain that the first peak ($\sim$700 nm) is governed by chlorophyll absorption, and that subsequent peaks are attributed to leaf scattering rather than to chlorophyll content.

### 6.2. Broadband vs. narrowband

The broadband (Landsat TM spectral bands) indices were first compared with their narrowband counterparts in terms of the relative REN difference defined in Eq. (25)

$$\%\mathrm{REN\ difference} = \frac{\mathrm{REN}_{\mathrm{Broad\ band\ VI}} - \mathrm{REN}_{\mathrm{Narrow\ band\ VI}}}{100}. \quad (25)$$

For LAI estimation, the comparison showed that, with the exception of TVI, the broadband indices were generally more sensitive to the pooled effects of illumination geometry, canopy architecture, and leaf biochemistry ($\theta_s$, MTA and $C_{ab}$). However, all broadband indices were more affected by the spectral properties of the background ($\rho_s(\lambda)$), whereas they were less affected by erroneous assumptions about the atmospheric composition ($\tau_{550}$ and $H_2O$).

For CCD estimation, the comparison showed that the broadband indices were less sensitive to the pooled effects of illumination geometry and canopy architecture ($\theta_s$ and

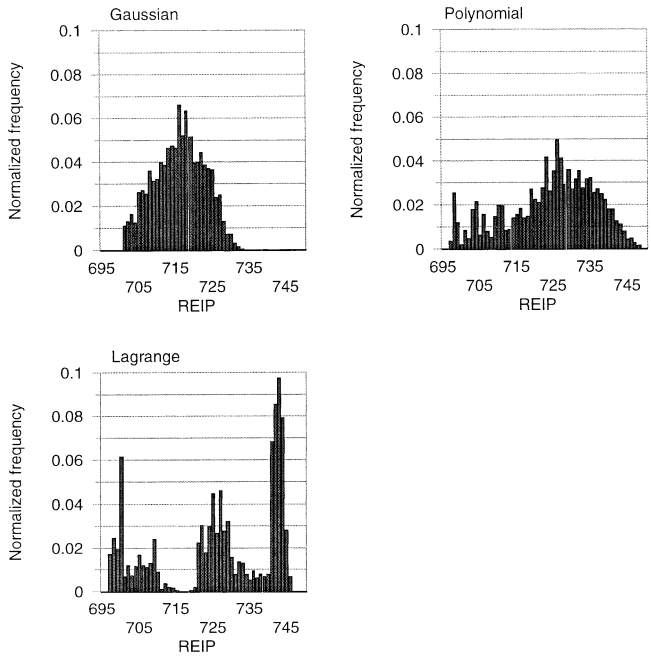


Fig. 3. The distribution of REIP calculated using (1) an inverted Gaussian model, (2) a sixth-order polynomial, and (3) Lagrangian interpolation applied to the first-derivative transformation of the reflectance spectrum. The calculations are based on the Database 1 data.

MTA). Further, the broadband indices were less sensitive to erroneous assumptions about the atmospheric composition ($\tau_{550}$ and $H_2O$), but more sensitive to the spectral properties of the background ($\rho_s(\lambda)$).

A comparative analysis of performance between hyperspectral indices and traditional indices will be influenced by the bandwidth of the spectral bands used to calculate the traditional indices. We chose to use the data set that showed the least dependence on the canopy parameters excluding the explanatory variable (LAI or CCD). As a result, the indices used for LAI prediction, except for TVI, were calculated from the narrowband data set, and the indices used for CCD prediction were calculated from the broadband data set.

### 6.3. Performance of the VIs

The VIs that we have dealt with in this study can be grouped into (1) Red–NIR indices, (2) Soil corrected Red-NIR indices, and (3) Indices based on the shape of the spectral reflectance curve from the green to the NIR derived from three or more discrete bands. The Group 1 indices are usually simple and easy to use, because the involved arithmetics are simple and no auxiliary information is required. However, these indices do not allow for adjustments to account for differences in the spectral properties of the background. The Group 2 indices have this flexibility. Richardson and Wiegand (1977) introduced the soil line concept by demonstrating that bare soil reflectance values in the Red and the Near-InfraRed wavelengths are linearly related. The Group 2 indices include soil line coefficients in their formulations. However, the slope and intercept of the *vegetation* isolines in Red–NIR space depend on both the spectral characteristics of the background (i.e. the soil line coefficients) and canopy density and architecture (Baret et al., 1989; Huete, 1989). In consequence, none of the indices belonging to Group 1 or 2 are insensitive to soil brightness effects (Fig. 2). Group 3 represents indices that in some way or another are related to the long wavelength absorption wing of the red chlorophyll pigment absorption band. This feature is directly coupled to the REIP (Collins, 1978), which has been shown to be related to vegetation density measures such as LAI and CCD (Boochs et al., 1997; Horler, Dockray, & Barber, 1983; Horler, Dockray, Barber, & Barringer, 1983; Miller et al., 1990). It will also have implications for indices based on measures of area across the chlorophyll absorption well. Demetriades-Shah et al. (1990) showed that the second derivative of vegetation reflectance spectra is independent of the spectral properties of the background, if the background reflectance varies linearly with the wavelength. This has been confirmed in a study by Baret et al. (1992) based on model simulations. They also showed that irradiance conditions (sun position and diffuse fraction) only had a minor influence on REIP. However, when indices are calculated from data recorded by high spectral resolution airborne or space-based sensors, the narrow atmospheric gaseous absorption bands may cause problems (Baret et al., 1992).

The relative magnitude of atmospheric scattering decreases with increasing wavelength (Kaufman, 1989). Since the reflectance of vegetation is low in the visible wavelengths because of absorption by chlorophyll, the radiance measured from a space-based platform will be dominated by path radiance. Thus, VIs calculated from such data will be sensitive to changes of atmospheric composition and should be corrected for atmospheric effects prior to comparative analyses. Jackson, Slater, and Pinter (1983) tested the effect of atmospheric turbidity on some of the Groups 1 and 2 indices and found that atmospheric path radiance affected all of the indices, but especially the ratio-based indices were found to be very sensitive to atmospheric path radiance.

#### 6.3.1. Prediction of LAI

The REN values associated with each VI for canopy, background, and atmospheric effects were calculated and graphed for different levels of LAI (Fig. 4a–d). The indices that were least affected by variations in canopy architecture and biochemistry as well as by the spectral properties of the background were SAVI2, RDVI, MSAVI2, and ATSAVI. The indices that were least affected by erroneous assumptions about atmospheric properties were CACI, DZ2_DGVI, PVI, TVI, DVI, and DZ1_DGVI. However, these indices all showed slightly higher dependence on the properties of the canopy and significantly higher dependence on the spectral properties of the background. The well-known RVI and NDVI were the best indices at low and medium LAIs, respectively. The CRCWD index also performed well at low to medium LAIs, but only marginally better than the much simpler NDVI, which is also considerably less sensitive to variations of the solar zenith angle (Fig. 6a–b). The very similar sensitivity patterns between CRCWD and NDVI and the sensitivity of CRCWD to solar zenith angle suggests using NDVI, because this index is widely known and much simpler to calculate.

In dense canopies characterized by high LAIs the best LAI estimator in terms of sensitivity to canopy effects was MSAVI2. However, this index is very sensitive to atmospheric effects. The CACI index provides an alternative if atmospheric effects are of concern. TVI is the broadband variant of the CACI index. A comparison between the performance of these two indices reveals that the standard error of the LAI estimate associated with canopy effects is only reduced by approximately 8% if CACI is replaced by TVI or DVI for high range LAI values (Fig. 4c).

It is interesting to note that the REIP measures all performed poorly to variations in the canopy. These results contradict the results of a previous study by Broge et al. (1997), which proved $REIP_{Gaus}$ to be better than NDVI for estimation of LAI. This suggests that the choice of VI for

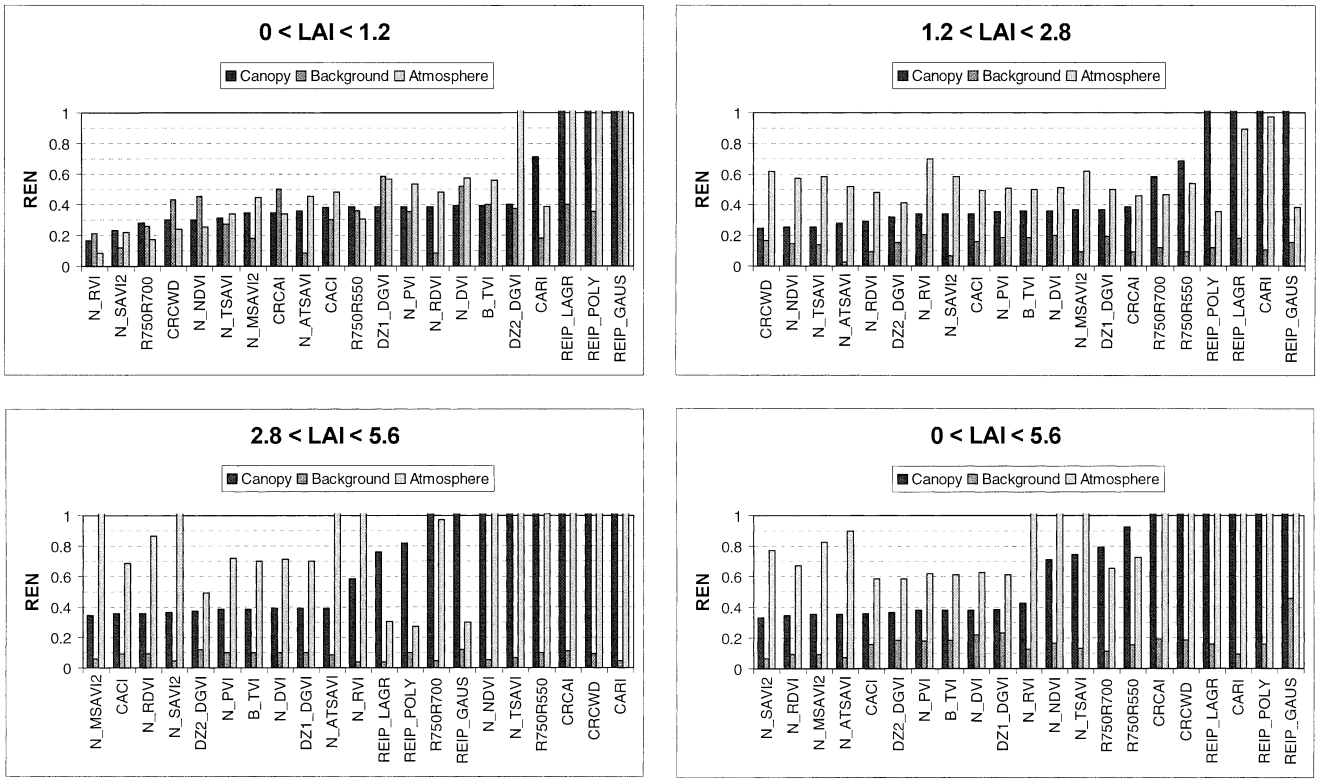


Fig. 4. (a–d) REN associated with estimation of LAI. REN is calculated for each index with respect to canopy, background, and atmospheric effects. The indices are listed from left towards right with increasing sensitivity to variations of MTA and $C_{ab}$.

a specific purpose should be based on a sensitivity analysis that only considers the range of parameters specific to the soil–vegetation system under investigation. For instance, the range in leaf chlorophyll content has been set to a factor 4, which is likely to be far too high for most cereal crops, whereas this range might be a reasonable choice if several different vegetation types are to be stratified using the same algorithm.

*6.3.2. Prediction of CCD*

For CCD prediction the situation is slightly different (Fig. 5a–d). Overall, the index that proved least affected by canopy variations was the simple broadband RVI. However, SAVI2 is a better choice when both soil background and atmospheric effects are of concern. Whereas the simpler ratio-based indices seem to be least affected by canopy and atmospheric variations at low CCD values, the novel CRCAI index proposed in this paper proved superior at midrange CCD values. The REIP calculated using the Lagrangian interpolation technique ($REIP_{Lagr}$) proved to be the best indicator of CCD in dense green vegetation when the general status of the soil–vegetation system and/or the atmospheric conditions are unknown.

Using the wavelength of maximum slope (REIP) at the canopy level has been reported to minimize effects of atmosphere (Baret et al., 1992) and background (Baret et al., 1992; Demetriades-Shah et al., 1990; Horler et al., 1983). Our results confirm this for high vegetation densities. However, at low vegetation densities our results show that REIP is highly sensitive not only to erroneous assumptions about the atmospheric composition, but also to structural and biochemical variations in the canopy.

It is interesting to note that the sequence of the REIP measures is consistent at all levels of LAI and CCD (Figs. 4a–c and 5a–c) in terms of REN induced by canopy effects. This suggests that the Lagrangian interpolation method is superior for determination of REIP for error-free data. However, this method will be relatively sensitive to the noise inherent in real spectral reflectance data sets. This is due to the fact that $REIP_{Lagr}$ is calculated from a narrow spectral window of three adjacent bands that are red- or blue-shifted across the red edge. The $REIP_{Gaus}$ and $REIP_{Poly}$ indices that are based on a function fitted to the reflectance of all 16 bands across the red edge region are less sensitive to variations of background and atmosphere. The reason for this is the built-in smoothing effect of these techniques and the fact that the spectral window of operation remains fixed. All the REIP measures proved to be relatively insensitive to variations in solar zenith angle (Fig. 6a), which is in agreement with the findings of other studies (Baret et al., 1992; Baret, Jacquemoud, Leprieur, & Guyot, 1990).

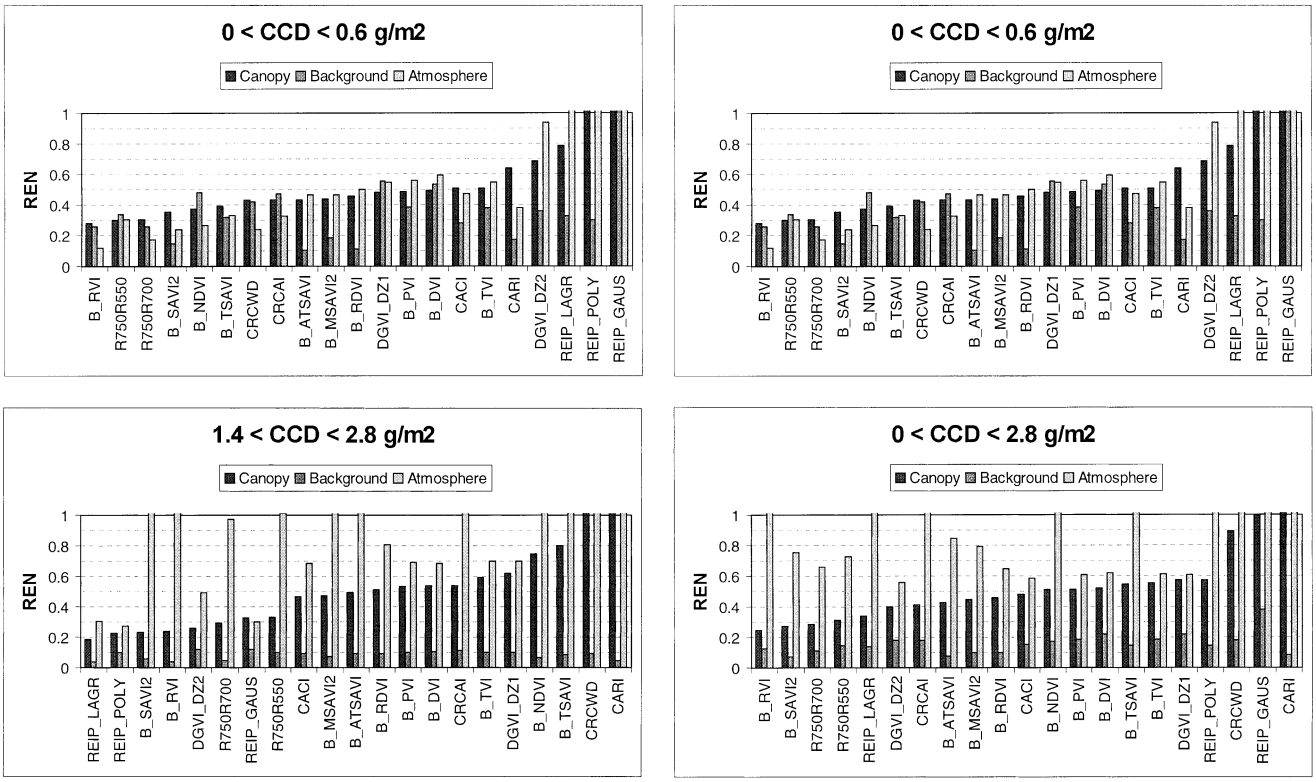


Fig. 5. (a–d) REN associated with estimation of CCD. REN is calculated for each index with respect to canopy, background, and atmospheric effects. The indices are listed from left towards right with increasing sensitivity to variations of MTA.

The proposed CRCWD index is highly sensitive to variations of the position of the sun. SAVI2 is generally least affected by variations in the solar geometry (Fig. 6b) whereas NDVI and the transformed SAVIs are considerably affected at low- and midrange LAI values and RVI is affected at high LAI values. The dependency of SAVI2 on solar angle is consistently low (Fig. 6b). This strengthens the position of SAVI2 as the best suited all-round index for estimation of LAI and CCD of homogenous green canopies.

## 7. Conclusion

Classic VIs based on broadband (TM sensor configuration) and narrow band (ideal 10 nm wide bands) reflectance data were compared. It was shown that the broadband indices were less affected by external factors when used as estimators of LAI or canopy chlorophyll content.

The performance of these indices was then compared with the performance of various hyperspectral indices, i.e. recently proposed indices that are based on narrow band

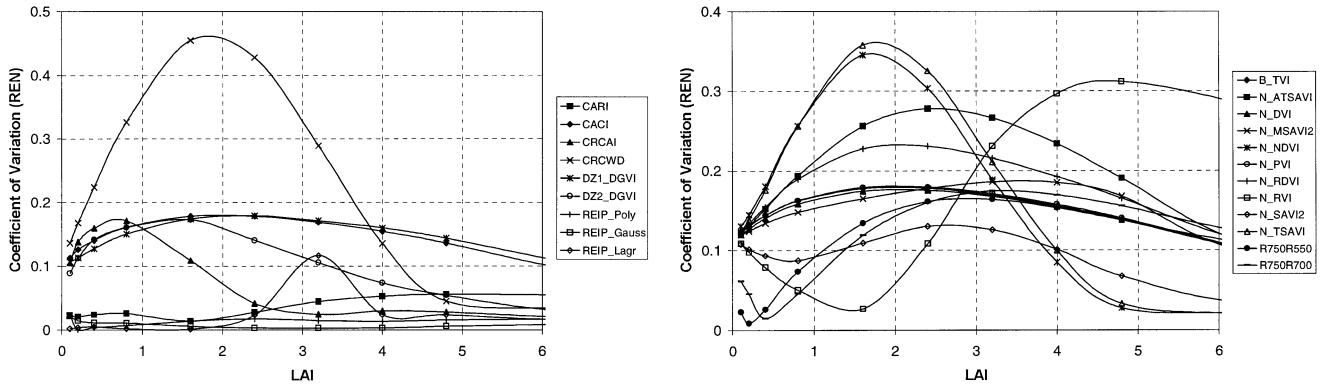


Fig. 6. (a–b) Sensitivity of the VIs to solar zenith angle variations. The sensitivity is expressed as the coefficient of variation of the REN value calculated at four different solar zenith angles ($\theta_s$=[15°, 30°, 45°, 60°]). The coefficient of variation of REN is calculated as the ratio of the standard deviation of REN to the average REN.

reflectance data. The classic broadband VIs generally seem to be slightly better at predicting LAI (Fig. 4d) and CCD (Fig. 5d) than the more recent narrowband indices, including the ones based on waveform analysis techniques.

Overall, the broadband SAVI2 index is least affected by background reflectance for both LAI and CCD estimation, and is also the best predictor of LAI. RVI is marginally better than SAVI2 for CCD estimation in terms of canopy effects, but it becomes increasingly sensitive to atmospheric effects and solar zenith angle with increasing vegetation densities. Further, SAVI2 proved to be least affected by illumination geometry changes.

RVI was the best estimator of both LAI and CCD for low vegetation densities, i.e. the least sensitive to variations in canopy structure or atmospheric composition, but ATSAVI was least sensitive to changes in background reflectance.

Continuum removal techniques applied to high resolution spectral reflectances across the red chlorophyll absorption band led to the development of two new VIs based on the area or depth of the convex hull spanned by the continuum removed spectra. These new indices proved to be the best estimators at medium range vegetation densities. The CRCAI index is superior for estimation of CCD in the midrange ($0.6 < \text{CCD(g Chl/ground m}^2) < 1.4$) if canopy properties are the major unknown (Fig. 5d). Likewise, the CRCWD index is the most accurate estimator of LAI in the midrange ($1.2 < \text{LAI} < 2.8$) under these conditions (Fig. 4d). However, the sensitivity pattern of NDVI is practically identical to that of CRCWD, which suggests that NDVI be used because of its simplicity compared with CRCWD.

The REIP indices proved surprisingly sensitive to variations of canopy parameters, background parameters, and atmospheric parameters. Only at high vegetation densities did the REIP indices perform well for estimation of CCD. The Lagrangian interpolation method gives the most accurate estimate of REIP. It is consistently the best of the three methods for estimation of LAI or CCD in terms of sensitivity to canopy effects, and the best overall estimator of CCD at high vegetation densities. LAI was best estimated by MSAVI2 at high vegetation densities. However, the area-based hyperspectral indices CACI and DZ2_DGVI provide an alternative if atmospheric effects are of concern.

The results indicate that hyperspectral indices based on various methods of waveform analysis or discrete narrowband ratios on and around the red edge region are not necessarily better predictors of LAI and CCD than the classic broadband indices considered in this study (Figs. 4a–d and 5a–d). However, one must bear in mind that this conclusion is based on the assumption that the SAIL + PROSPECT model can accurately describe the radiative regime in a canopy, and that this canopy fulfil the assumptions of the SAIL model regarding homogeneity of the canopy and azimuthally uniform leaf orientation. Further, the presented results are biased by the choice of input parameters for each of the databases. This kind of analysis should therefore be designed to match the specific conditions of the soil–vegetation system under investigation. The range of each of the bio-physical parameters used as input for the simulations should be carefully selected based on a priori knowledge of extremes encountered by phenological evolution, climatic factors, or other external parameters affecting the system, thus providing the optimal foundation for the selection of the most suitable VI.

The results reported in this paper are derived from an analysis of simulated reflectance data, i.e. data that are free of noise. Measured data are usually noisy due to signal amplification, binary encoding, etc. While it was not the purpose of this study to assess the effects of measurement-related noise, it may be an important factor depending on the sensor system, vegetation status, and illumination conditions. Future works should consider establishment of functions to calculate sensor-specific spectral signal-to-noise ratios for various conditions. This will allow effects of sensor-related noise to be included in this kind of analysis. It could be facilitated simply by adding a Gaussian distributed noise component with zero mean and variance equal to the modelled signal-to-noise to each reflectance value in the simulated spectra.

## Acknowledgments

The authors are indebted to Dr. Craig S.T. Daughtry (ARS-USDA) for facilitating our use of the soil reflectance database, and to Dr. Stephane Jacquemoud (University of Paris) for supplying the code for the SAIL + PROSPECT model.

## References

Baret, F., Champion, I., Guyot, G., & Podaire, A. (1987). Monitoring wheat canopies with a high spectral resolution radiometer. *Remote Sensing of the Environment*, *22*, 367–378.

Baret, F., & Guyot, G. (1991). Potentials and limits of vegetation indices for LAI and APAR assessment. *Remote Sensing of the Environment*, *35*, 161–173.

Baret, F., Guyot, G., & Major, D. J. (1989). TSAVI: a vegetation index which minimizes soil brightness effects on LAI and APAR estimation. In: *Proc. IGARRS '89. 12th Canadian Symposium on Remote Sensing,* (vol. 3, pp. 1355–1358). Vancouver, Canada, p. 4 (10–14 July).

Baret, F., Jacquemoud, S., Guyot, G., & Leprieur, C. (1992). Modelled analysis of the biophysical nature of spectral shifts and comparison with information content of broad bands. *Remote Sensing of the Environment*, *41*, 133–142.

Baret, F., Jacquemoud, S., Leprieur, C., & Guyot, G. (1990). Are the spectral shifts an operational concept? — Critical analysis of theoretical and experimental results. In: *Proc. Airborne Geoscience Workshop, 4–5 June*, Jet Propulsion Laboratory, California Institute of Technology Pasadena, CA, USA (pp. 58–71).

Ben-dor, E., & Kruse, F. A. (1995). Surface mineral mapping of Makhtesh Ramon, Negev, Israel using GER 63 channel scanner data. *International Journal of Remote Sensing*, *16*, 3529–3553.

Bonham-Carter, G. F. (1988). Numerical procedures and computer program for fitting an inverted Gaussian model to vegetation reflectance data. *Computer & Geosciences*, *14*, 339–356.

Boochs, F., Kupfer, G., Dockter, K., & Kühbach, W. (1997). Shape of the red edge as vitality indicator for plants. *International Journal of Remote Sensing*, *11*, 1741–1753.

Broge, N. H., Hvidberg, M., Hansen, B. U., Andersen, H. S., & Nielsen, A. A. (1997). Analysis of spectral–biophysical relationships for a wheat canopy. In: *Proc. Third International Airborne Remote Sensing Conference and Exhibition* (vol. II pp. 373–379). Copenhagen, Denmark, 7–10 July. Erim International, Inc., Ann Arbor, Michigan, USA.

BSC (Better Solutions Consulting Limited Liability). ENVI User's Guide. July 1999 edition.

Clevers, J.G.P.W. (1989). The application of a weighted infra-red vegetation index for estimating leaf area index by correcting for soil moisture. *Remote Sensing of the Environment*, *29*, 25–37.

Collins, W. (1978). Remote sensing of crop type and maturity. *Photogrammetric Engineering and Remote Sensing*, *26*, 43–55.

Daughtry, C. S. T., McMurtrey, J. E. III, Kim, M. S., & Chappelle, E. W. (1996). Estimating crop residue cover by blue fluorescence imaging. *Remote Sensing of the Environment*, *60*, 14–21.

Dawson, T. P., & Curran, P. J. (1998). A new technique for interpolating the red edge position. *International Journal of Remote Sensing*, *19*, 2133–2139.

Demetriades-Shah, T. H., Steven, M. D., & Clark, J. A. (1990). High resolution derivative spectra in remote sensing. *Remote Sensing of the Environment*, *33*, 55–64.

Elvidge, C. D., & Chen, Z. (1995). Comparison of broad-band and narrow-band red and near-infrared vegetation indices. *Remote Sensing of the Environment*, *54*, 38–48.

Gilabert, M. A., Gandia, S., & Melia, J. (1996). Analyses of spectral–biophysical relationships for a corn canopy. *Remote Sensing of the Environment*, *55*, 11–20.

Gitelson, A. A., Merzlyak, M. N., & Lichtenthaler, H. K. (1996). Detection of red edge position and chlorophyll content by reflectance measurements near 700 nm. *Journal of Plant Physiology*, *148*, 501–508.

Goel, N. S., & Thompson, R. L. (1984). Inversion of vegetation canopy reflectance models for estimating agronomic variables: IV. Total inversion of the sail model. *Remote Sensing of the Environment*, *15*, 237–253.

Guyot, G., Baret, F., & Jacquemoud, S. (1989). Imaging spectroscopy for vegetation studies. In: F. Toselli, & J. Bodechtel (Eds.), *Imaging spectroscopy: fundamentals and prospective applications* (pp. 145–165). Kluwer Academic Publishers, Dordrecht.

Hall, D. O., & Rao, K. K. (1987). *Photosynthesis* (4th ed.). Great Britain: Edward Arnold.

Holben, B. N., Eck, T. F., Slutsker, I., Tanre, D., Buis, J. P., Setzer, A., Vermote, E., Reagan, J. A., Kaufman, Y. J., Nakajima, T., Lavenu, F., Jankowiac, I., & Smirnow, A. (1998). AERONET — a federated instrument network and data archive for aerosol characterization. *Remote Sensing of the Environment*, *66*, 1–16.

Horler, D. N. H., Dockray, M., & Barber, J. (1983). The red edge of plant leaf reflectance. *International Journal of Remote Sensing*, *4*, 273–288.

Horler, D. N. H., Dockray, M., Barber, J., & Barringer, A. R. (1983). Red edge measurements for remotely sensing plant chlorophyll content. *Advances in Space Research*, *3*, 273–277.

Huete, A. R. (1988). A Soil-Adjusted Vegetation Index (SAVI). *Remote Sensing of the Environment*, *25*, 295–309.

Huete, A. R. (1989). Soil influences in remotely sensed vegetation-canopy spectra. In: G. Asrar (Ed.), *Theory and applications of optical remote sensing* (pp. 107–141). New York: Wiley.

Huete, A. R., & Jackson, R. D. (1988). Soil and atmosphere influences on the spectra of partial canopies. *Remote Sensing of the Environment*, *25*, 89–105.

Huete, A. R., Jackson, R. D., & Post, D. F. (1985). Spectral response of a plant canopy with different soil backgrounds. *Remote Sensing of the Environment*, *17*, 37–53.

Jackson, R. D., & Pinter, P. J. Jr. (1986). Spectral response of architecturally different wheat canopies. *Remote Sensing of the Environment*, *20*, 43–56.

Jackson, R. D., Slater, P. N., & Pinter, P. J. (1983). Discrimination of growth and water stress in wheat by various vegetation indices through clear and turbid atmospheres. *Remote Sensing of the Environment*, *13*, 187–208.

Jacquemoud, S. (1993). Inversion of the PROSPECT + SAIL canopy reflectance model from AVIRIS equivalent spectra: theoretical study. *Remote Sensing of the Environment*, *44*, 281–292.

Jacquemoud, S., & Baret, F. (1990). PROSPECT: a model of leaf optical properties spectra. *Remote Sensing of the Environment*, *34*, 75–91.

Jacquemoud, S., Baret, F., Andrieu, B., Danson, F. M., & Jaggard, K. (1995). Extraction of vegetation biophysical parameters by inversion of the PROSPECT + SAIL models on sugar beet canopy reflectance data. Application to TM and AVIRIS sensors. *Remote Sensing of the Environment*, *52*, 163–172.

Jacquemoud, S., Ustin, S. L., Verdebout, J., Schmuck, G., Andreoli, G., & Hosgood, B. (1996). Estimating leaf biochemistry using the PROSPECT leaf optical properties model. *Remote Sensing of the Environment*, *56*, 194–202.

Jordan, C. F. (1969). Derivation of leaf area index from quality of light on the forest floor. *Ecology*, *50*, 663–666.

Kaufman, Y. J. (1989). The atmospheric effect on remote sensing and its correction. In: G. Asrar (Ed.), *Theory and applications of optical remote sensing* (pp. 336–428). New York: Wiley.

Kim, M. S., Daughtry, C. S. T., Chappelle, E. W., & McMurtrey, J. E. (1994). The use of high spectral resolution bands for estimating absorbed photosynthetically active radiation (APAR). In: *Proc. ISPRS'94, Val d'Isere, France* 17–21 January 1994 (pp. 299–306).

Kruse, F. A. (1988). Use of airborne imaging spectrometer data to map minerals associated with hydrothermally altered rocks in the Northern Grapevine Mountains, Nevada, and California. *Remote Sensing of the Environment*, *24*, 31–51.

Kuusk, A. (1991). The hot spot effect in plant canopy reflectance, Chapter 2. In: R. Ross, & R. Myneni (Eds.), *Photon vegetation interactions. Applications in optical remote sensing and plant ecology* (pp. 139–159). Berlin: Springer.

Lichtenthaler, H. K., Gitelson, A. A., & Lang, M. (1996). Non destructive determination of chlorophyll content of leaves of a green and an aurea mutant of tobacco by reflectance measurements. *Journal of Plant Physiology*, *148*, 483–493.

Major, D. J., Baret, F., & Guyot, G. (1990). A ratio vegetation index adjusted for soil brightness. *International Journal of Remote Sensing*, *11*, 727–740.

Marquardt, D. W. (1963). An algorithm for least squares estimation of nonlinear parameters. *Journal for the Society of Industrial and Applied Mathematics*, *11*, 431–441.

Mauser, W., & Bach, H. (1995). Imaging spectroscopy in hydrology and agriculture — determination of model parameters. In: J. Hill, & J. Megier (Eds.), *Imaging spectrometry — a tool for environmental observations* (pp. 261–283). Dordrecht, The Netherlands: Kluwer Academic Publishers.

McClatchey, R. A., Fenn, R. W., Selby, J. E. A., Volz, F. E., & Garing, J. S. (1971). Optical properties of the atmosphere. *Environment Research Papers*, *354*.

McClatchey, R. A., Fenn, R. W., Selby, J. E. A., Volz, F. E., & Garing, J. S. (1972). Optical properties of the atmosphere (3rd ed.). AFCRh Environ. Res. Papers No. 411 108pp.

Miller, J. R., Hare, E. V., & Wu, J. (1990). Quantitative characterization of the vegetation red edge reflectance. *International Journal of Remote Sensing*, *11*, 1755–1773.

Myneni, R. B., & Williams, D. L. (1994). On the relationship between FAPAR and NDVI. *Remote Sensing of the Environment*, *49*, 200–211.

Pearson, R. L., & Miller, L. D. (1972). *Remote mapping of standing crop biomass for estimation of the productivity of the short-grass prairie, Pawnee National Grasslands, Colorado* (pp. 1357–1381). Ann Arbor, MI: ERIM.

Pinter, P. J. Jr., Jackson, R. D., Ezra, C. E., & Gausman, H. W. (1985). Sun-angle and canopy-architecture effects on the spectral reflectance of six wheat cultivars. *International Journal of Remote Sensing*, *6*, 1813–1825.

Press, W. H., Flannery, B. P., Teukolsky, S. A., & Vetterling, W. T. (1989). Numerical recipes in Pascal. In: W. H. Press, B. P. Flannery, S. A. Teukolsky, & W. T. Vetterling (Eds.), *The art of scientific computing*. Cambridge: Cambridge Univ. Press (759 pp.).

Qi, J., Chehbouni, A., Huete, A. R., Kerr, Y. H., & Sorooshian, S. (1994). A modified soil adjusted vegetation index. *Remote Sensing of the Environment*, *48*, 119–126.

Richardson, A. J., & Wiegand, C. L. (1977). Distinguishing vegetation from soil background information. *Photogrammetric Engineering and Remote Sensing*, *43*, 1541–1552.

Roujean, J. L., & Breon, F. M. (1995). Estimating PAR absorbed by vegetation from bidirectional reflectance measurements. *Remote Sensing of the Environment*, *51*, 375–384.

Rouse, J. W., Haas, R. H., Schell, J. A., Deering, D. W., & Harlan, J. C. (1974). *Monitoring the vernal advancement of retrogradation of natural vegetation*. NASA/GSFC, Type III, Final Report, Greenbelt, MD, USA, pp. 1–371.

Slater, P. N., & Jackson, R. D. (1982). Atmospheric effect on radiation reflected from soil and vegetation as measured by orbiting sensors using various scanning directions. *Applied Optics*, *21*, 3923–3931.

Thomas, J. R., & Gausman, H. W. (1977). Leaf reflectance vs. leaf chlorophyll and cartenoid concentrations for eight crops. *Agronomy Journal*, *69*, 799–802.

Verhoef, W. (1984). Light scattering by leaf layers with application to canopy reflectance modeling: the SAIL model. *Remote Sensing of the Environment*, *16*, 125–141.

Vermote, E., Tanre, D., Deuze, J. L., Herman, M., & Morcrette, J. J. (1996). *6S User Guide*, version 1, October 7, 1996 (unpublished).

Wiegand, C. L., Maas, S. J., Aase, J. K., Hatfield, J. L., Pinter, P. J. Jr., Jackson, R. D., Kanemasu, E. T., & Lapitan, R. L. (1992). Multisite analyses of spectral–biophysical data for wheat. *Remote Sensing of the Environment*, *42*, 1–21.